AD-770 009

IR WINDOW STUDIES

Ferdinand Kroger, et al

University of Southern California

Prepared for:

Air Force Cambridge Research Laboratories

15 June 1973

DISTRIBUTED BY:

AD 770 009

## DOCUMENT CONTROL DATA - R & D

*(Security classification of title, body of abstract and indexing annotation must be entered when the overall report is classified)*

| 1. ORIGINATING ACTIVITY *(Corporate author)* | 2a. REPORT SECURITY CLASSIFICATION |
|---|---|
| Electronic Sciences Laboratory | UNCLASSIFIED |
| University of Southern California | 2b. GROUP |
| Los Angeles, California 90007 | |

**3. REPORT TITLE**

IR WINDOW STUDIES

**4. DESCRIPTIVE NOTES** *(Type of report and inclusive dates)*

Scientific          Interim.

**5. AUTHOR(S)** *(First name, middle initial, last name)*

Ferdinand Kröger and
John H. Marburger

| 6. REPORT DATE | 7a. TOTAL NO. OF PAGES | 7b. NO. OF REFS |
|---|---|---|
| 15 June 1973 | ~~56~~ 65 | 21 |
| 8a. CONTRACT OR GRANT NO | 9a. ORIGINATOR'S REPORT NUMBER(S) | |
| F19628-72-C-0275 | | |
| b. PROJECT NO  Task, Work Units Nos. | Quarterly Technical Report No. 4 | |
| 2055    n/a          n/a | | |
| c. DoD Element 61101 D | 9b. OTHER REPORT NO(S) *(Any other numbers that may be assigned this report)* | |
| d. DoD Subelement n/a | AFCRL-TR-73-0414 | |

**10. DISTRIBUTION STATEMENT**

A-Approved for public release; distribution unlimited

| 11. SUPPLEMENTARY NOTES | 12. SPONSORING MILITARY ACTIVITY |
|---|---|
| TECH, OTHER | Air Force Cambridge Research Laboratories (LQ) |
| | L. G. Hanscom Field |
| | Bedford, Massachusetts 01730 |

**13. ABSTRACT**

Continuing wavelength dependent absorption measurements of "high purity" GaAs grown from the melt by a variety of techniques show remarkably similar structure in all samples. There appears to be a definite lower limit of about $\beta \approx .008$ cm$^{-1}$ at 10.6 $\mu$m for melt grown GaAs. Wide band emissivity measurements performed by Stierwalt (NELC, San Diego) agree well with our data, except for a small shift of scale attributable to a difference in ambient temperature. Preliminary measurements of the dielectric constant of GaAs have been obtained. A systematic study of diffuse intensity streaks in the electron diffraction pattern of GaAs single crystals indicates that they are of thermal origin, and do not arise from inclusions or impurities. The absorption coefficient of a good quality sample of GaAs has been reduced to that of best quality samples by annealing. Greatest reduction occurred in the 9.5 $\mu$m feature common to all melt grown samples measured. High purity KCl crystals have been grown, and preparations are now being made for the growth of OH$^-$ doped KCl and high purity KBr. Experiments on self diffusion of Cd and Te, and high temperature Hall effect in CdTe and In-doped CdTe have been completed. Experiments have been performed to determine 10.6 $\mu$m absorption in highly absorbing material (quartz) using acoustical surface wave techniques. The data require numerical analysis (now in progress) to extract the absorption coefficient. An analysis of the influence of stress induced birefringence on thermal slewing of acentric beams has been substantially complete.

i.

65

DD FORM 1473
1 NOV 65

| 14 KEY WORDS | LINK A | | LINK B | | LINK C | |
|---|---|---|---|---|---|---|
| | ROLE | WT | ROLE | WT | ROLE | WT |
| IR Windows | | | | | | |
| Alkali Halides | | | | | | |
| III-V Semiconductors | | | | | | |
| II-VI Semiconductors | | | | | | |
| Thermal lensing | | | | | | |
| IR absorption | | | | | | |

# IR WINDOW STUDIES

by

Ferdinand A. Kröger

and

John H. Marburger

Electronic Sciences Laboratory
School of Engineering
University of Southern California
Los Angeles, California 90007

Quarterly Technical Report No. 4

15 June 1973

iii.

iv.

# ABSTRACT

Continuing wavelength dependent absorption measurements of "high purity" GaAs grown from the melt by a variety of techniques show remarkably similar structure in all samples. There appears to be a definite lower limit of about $\beta \approx .008$ cm$^{-1}$ at 10.6 $\mu$m for melt grown GaAs. Wide band emissivity measurements performed by Stierwalt (NELC San Diego) agree well with our data, except for a small shift of scale attributable to a difference in ambient temperature. Preliminary measurements of the dielectric constant of GaAs have been obtained. A systematic study of diffuse intensity streaks in the electron diffraction pattern of GaAs single crystals indicates that they are of thermal origin, and do not arise from inclusions or impurities. The absorption coefficient of a good quality sample of GaAs has been reduced to that of best quality samples by annealing. Greatest reduction occurred in the 9.5$\mu$m feature common to all melt grown samples measured. High purity KCl crystals have been grown, and preparations are now being made for the growth of OH$^-$ doped KCl and high purity KBr. Experiments on self diffusion of Cd and Te, and high temperature Hall effect in CdTe and In-doped CdTe have been completed. Experiments have been performed to determine 10.6 $\mu$m absorption in a highly absorbing material (quartz) using acoustical surface wave techniques. The data require numerical analysis (now in progress) to extract the absorption coefficient. An analysis of the influence of stress induced birefringence on thermal slewing of acentric beams has been substantially completed.

1

# CONTENTS

1.                          INTRODUCTION


        The format of this report follows closely that of the first quarterly
report in which projects are identified by codes keyed to the contract
work statement.

The various categories are briefly:

    a)   Crystal growth
    b)   Polycrystalline window fabrication
    c)   Mechanical properties of window materials
    d)   Window material defect characterization
    e)   Theory of residual IR optical absorption
    f)   Absorption measurement techniques
    g)   Theoretical evaluation of optical performances of
         windows

a.1    Effect of Oxygen and Other Impurities on IR Absorption in II-VI and
III-V Compounds

James M. Whelan

## A. GaAs Epitaxial Growth-Horizonal Reactor

The apparatus has been completed and is presently being outgassed.
It will be available during the next quarter. Screening examinations were in
part responsible for the fact that film growth was delayed.

## B.   GaAs-Oxygen Studies

Progress was delayed because of a (successful) Ph. D. qualifying exami-
nation. Most of the work this quarter was spent on evaluating the zirconia
electrolytic cell as a means of establishing the relationship between the fugacity
of oxygen as a function of the atomic fraction of oxygen dissolved in gallium at
$500^\circ$C. This information is needed to develop a means for measuring oxygen
in GaAs and other materials. Difficulties in identifying the extent of hydrogen
ion diffusion in the zirconia have introduced an uncertainty in the above relation-
ship. Our preliminary one at $500^\circ$C is:

$$P^{\frac{1}{2}}(O_2) - 1.4 \times 10^{-11} \; \chi(O) \; atm^{-\frac{1}{2}} \; \text{where}$$

$P(O_2)$ is the effective oxygen pressure in equilibrium with a gallium solution
in which the atomic fraction of oxygen is $\chi(O)$. This is f r values of $\chi(O) \leq 10^{-6}$.
Preliminary indications are that the value of the constant is not strongly tempe-
rature dependent and that uncertainties in the interpretation of cell emf data are
substantially less at $600^\circ$C.

## a.2    Optimization of Alkali Halide Window Materials

Paul J. Shlichta, R. E. Chaney

Single crystals of KCl, purified by ion-exchange and treatment with HCl and $Cl_2$, have been grown by the procedures described in previous reports. The infrared absorption of these crystals is now being studied by laser calorimetry and low-temperature spectrophotometry; results will be tabulated in the next report.

Preparations are now underway for the growth of KCl crystals containing $OH^-$ ions. Two methods of doping will be used; (1) introducing KOH into the molten KCl and (2) exposing the molten salt and/or grown crystals to water vapor. These cyrstals will also be studied by calorimetry and infrared spectrophotometry.

Preparations are also being made for the growth of purified KBr crystals. Additional ion-exchange columns have been assembled and gas-handling systems have been installed for treatment of the molten KBr with HBr and $Br_2$. This facility should be operational sometime during the next quarter.

a.3 GROWTH OF CRYSTALS FOR IR WINDOW RESEARCH

E. A. Miller and W. R. Wilcox

(Chemical Vapor Deposition of Bulk Gallium Arsenide)

Work during this quarter was directed toward growth of bulk gallium
arsenide by the open tube chemical vapor deposition method using $AsCl_3$,
gallium and hydrogen. Results are summarized in Table I.

The all-glass system with furnace temperature control to $\pm$ $2^O$C was
placed in operation on schedule. Substrates used in this series of
experiments were GaAs oriented (100) $2^O$ off toward (110) and were
tellurium doped in the range of $5 \times 10^{17}$ to $2 \times 10^{18}$ atoms. The usual
cleaning and preparation procedure was as follows: The wafers were
mechanically polished to a bright mirror finish and then lightly etched in
5:1:1 $H_2SO_4$:$H_2O_2$:$H_2O$ for 10 minutes to remove traces of polishing com-
pounds and damage. Then substrates were rinsed in $H_2O$, methanol, and
dried in a stream of nitrogen. The substrates were then etched at $900^O$C
in the reactor just before deposition at $740-780^O$C.

The first few runs accomplished only etching of the substrate.
Attempts were made to modify the vapor composition in the region of the
substrate in the hope of arriving at the proper conditions for growth.
One possible solution involved a modified Ga source holder consisting of the
thermocouple-well extending only to the upstream end of the Ga melt. This
should have allowed much better vapor contact with the Ga melt. However,
negative results were obtained. Another modification was placement of
quartz discs in the tube near the Ga source and substrate to cut down on
free convection of the depositing species. This resulted in an amporhous

6

TABLE 1.   SUMMARY OF GaAs CVD RUNS
(3/1/73 - 5/31/73)

| Run No. | $H_2$ flow thru AsCl$_3$ | $H_2$ dilution flow | Substrate temperature | Major change to system | Results |
|---|---|---|---|---|---|
| CVD #6 | 60 cc/min | 140 cc/min | 750°C | All glass system. | Etched substrate. |
| CVD #7 | 60 cc/min | 140 cc/min | 750°C | T.C. clear from gallium chamber. | Etched substrate. |
| CVD #8 | 60 cc/min | 120 cc/min | 750°C | Baffles to cut down free convection. | Amorphous deposit. |
| CVD #9 | 60 cc/min | 120 cc/min | 750°C | Flushed system with H$_2$ 16 hours prior to run. | Etched substrate. |
| CVD #10 | 60 cc/min | 120 cc/min | 750°C | Increased temperature gradient in region of substrate. | Amorphous deposit. |
| CVD #11 | 120 cc/min | 240 cc/min | 750°C | Doubled total flow rate. | Severe etching of substrate. |
| CVD #12 | 120 cc/min | 120 cc/min | 760°C | Long furnace, open Ga boat. | Slight deposit, large Ga droplets formed. |
| CVD #13 | 120 cc/min | 120 cc/min | 750°C | Temperature profile as reported in the literature. | Growth with many hillocks. |
| CVD #14 | 120 cc/min | 120 cc/min | 750°C | Palladium diffused H$_2$ now. | Etched substrate. |
| CVD #15 | 120 cc/min | 120 cc/min | 750°C | Substrate cover during Ga melt saturation. | Good growth, specular deposit, fewer hillocks. |
| CVD #16 | 120 cc/min | 120 cc/min | 770°C | {111} A and B and {100} substrates constant temperature for AsCl$_3$ bubbler. | Good growth, uniformly rough deposit on {111} A substrate. |
| CVD #17 | 120 cc/min | 120 cc/min | 750°C | Five-day run, {111} A substrate. | Severe dendritic growth, substrate etched slightly. |

7

appearing GaAs deposit. Doubling the gas flow rate had no noticeable effect.

Deposition conditions on {100} oriented substrates proved to be much more critical than on previously-tested {111} A and B substrates. Therefore we proceeded to modify the system by obtaining a longer furnace and establishing a temperature gradient that was reported to give good results on {100} substrates with this $AsCl_3$, Ga system.[*] Figure 1 shows the temperature profile established in this furnace. This new system had a smaller diameter tube (40 mm I.D.) and an open boat inserted into the tube for the gallium source. The hydrogen flow through the $AsCl_3$ bubbler was usually 120 cc/min and the hydrogen dilution flow was also 120 cc/min. A palladium-diffusion hydrogen-purification system was also installed. A temperature controller held the temperature of the $AsCl_3$ bubbler to $\pm$ 0.1$^o$C. In subsequent runs we located the substrate in the tube near the best appearing GaAs wall deposits from preceding runs, although this position shifted slightly from run to run. Finally, we were successful and obtained about 20 μm of growth on a {100} substrate in 24 hours. Many growth hillocks were found on the surface.

We achieved better results when the substrates were placed under a cover during saturation of the gallium melt prior to deposition. We believe that without a cover GaCl disproportionates on the substrate to $GaCl_3$ and metallic gallium. The Ga on the substrate then acts as a preferred site for hillock and whisker formation by a vapor-liquid-solid

---

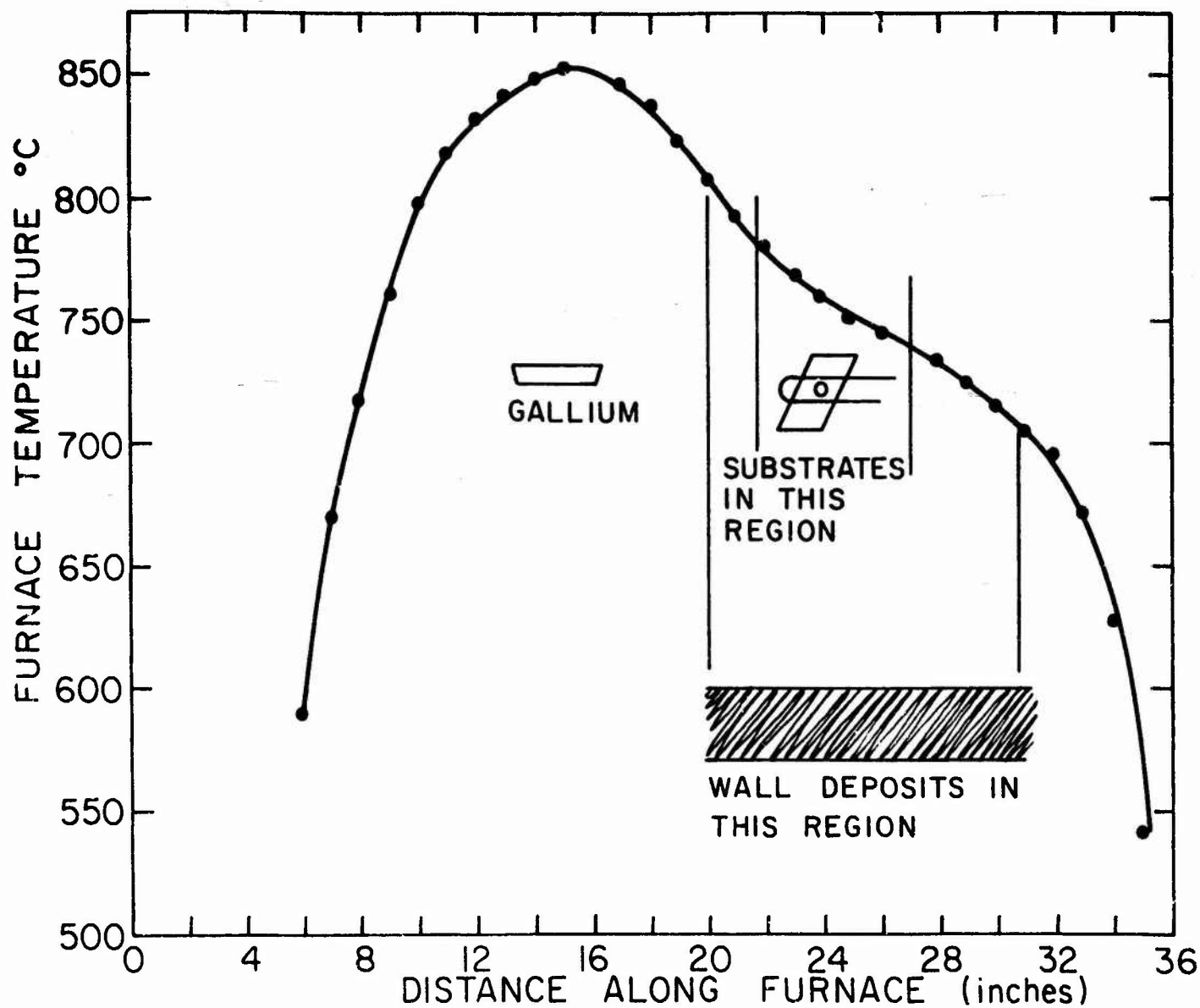[*] Wolfe, C.M., and Foyt, A.G., Electrochem. Tech., 6, 208 (1968).

Figure 1. Temperature profile in GaAs CVD system

growth mechanism.  In Figure 2 a portion of the substrate in a hillock free region is shown.  Figure 3 and 4 demonstrate typical hillock formation on these {100} substrates.  (Note the four-fold symmetry.) These surfaces, in spite of the imperfections, appear highly specular.

The next 24-hour run consisted of a {111} A and B twin substrate along with a {100} substrate.  The growth rate on the {111} A surface was much larger and rougher than on the {111} B and {100}, as expected. Figure 5 shows the result of this run.  Note the uniformly rough but hillock-free surface, approximately 250 μm thick.  This growth, even though rough, would be suitable for absorption measurements since such a rough surface could be easily polished mechanically.

Next we attempted to produce a deposit 1 to 2 mm thick over five days on a {111} A substrate.  The results were poor - slight etching of the substrate was even observed.  An overgrowth of large dendrites covered the area above the substrate.  We also noted large periodic fluctuations ($\sim 30^{\circ}$C) of substrate temperature every 12 to 13 hours, probably due to line voltage fluctuations.  The wall deposits appeared better upstream from the substrate.  This has been observed before -- when the substrate is placed in the region previously showing good wall deposits, the wall deposits now appear better in another region.

We plan to install constant voltage transformers for the power controllers to eliminate the temperature fluctuation problem.  A longer substrate holder and cover that will hold up to five samples is being built.  Hopefully under any given set of conditions a deposit suitable for absorption measurement can be grown thereby.
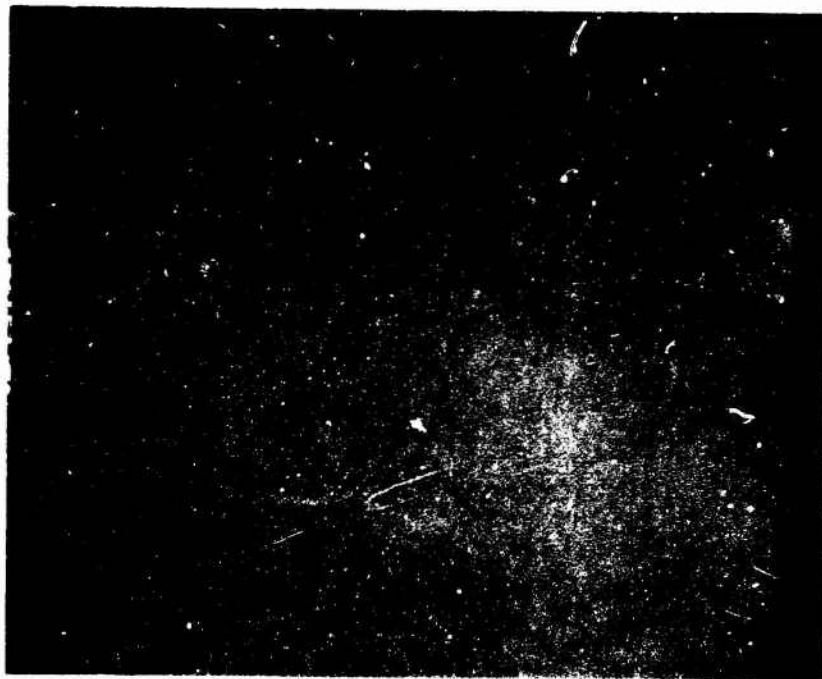
10

Figure 2. Scanning electron micrograph of deposit on
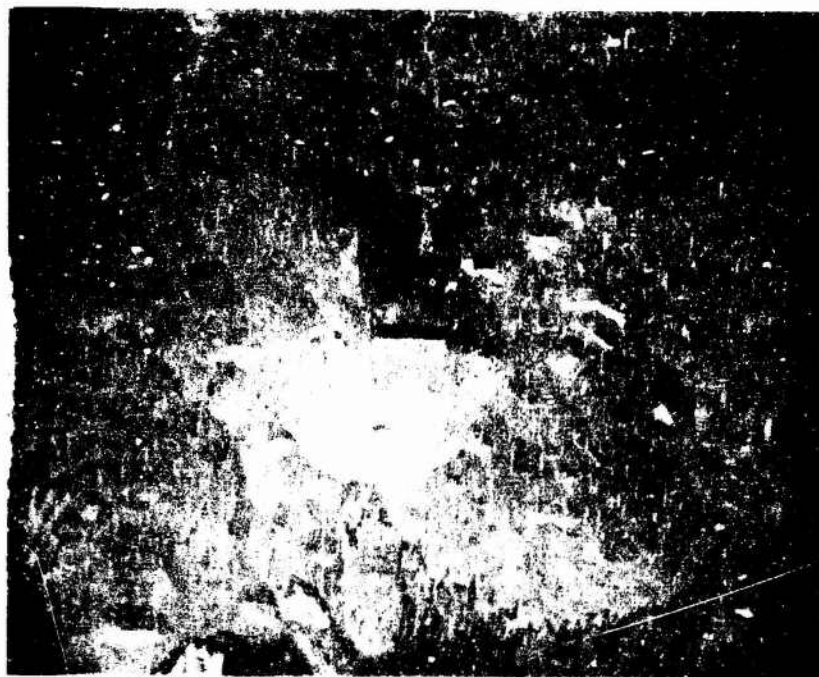(100) substrate. CVD-15. 50 X.



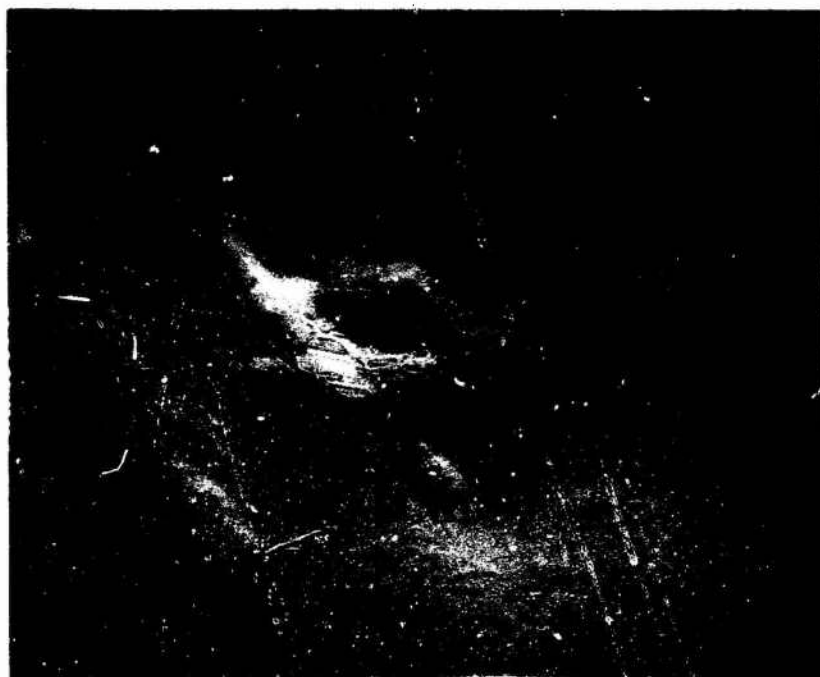Figure 3. Hillocks on deposit on (100) substrate.
CVD-15. 50 X.

11

Figure 4. Scanning electron micrograph of CVD-16.
200 X.



Figure 5. Deposit on {111} A and B twinned substrate,
showing greater deposit thickness on {111}
A face on left.

b.1.  Fabrication of Polycrystalline IR Window Materials

S. M. Copley, J. M. Whelan and V. Rana

Hot Press

The hot press and its operation have been described in the previous
quarterly reports.  The hot press has been constructed and tests are underway
to prepare it for operation.

As explained in earlier reports, the use of liquid arsenic as a sintering
aid in the hot pressing of GaAs powder, is made possible by containing it in
the die with a glass seal backed up by a suitable pressure of argon gas.  The
use of an inert atmosphere is required to prevent the graphite die and the
molybdenum chill from oxidizing.  In order to evacuate the hot press chamber
before introducing the argon gas, the chamber is connected to a vacuum system
consisting of a mechanical pump and a cold trap.  It is inevitable that there are
a large number of joints present in the system.  After a considerable amount of
leak testing and repairing, it is now possible to maintain a vacuum of 70 μ of
Hg or better in the hot press chamber with the mechanical pump isolated.
Considerable time has also been spent this period calibrating the thermocouples
and determining temperature profiles in the die obtained by adjustment of the
flow rate of cooling water to the molybdenum chill.

Since this hot press can be used for compacting powders of semiconductor
materials other than GaAs, initial experiments have been planned for compacting
CdTe powder.  CdTe has been obtained for this purpose from II-VI, Incorporated.[*]
In this case liquid Cd will be utilized as a sintering aid.  Unlike GaAs, compaction
of CdTe can be done under one atmosphere pressure of the argon gas.

Powders

One of the major difficulties in producing a transparent compact, is obtaining
powders of the semiconductor materials in the submicron size range.  In the
initial experiments, which are planned only to check the efficiency of the sintering
process, ball milled powder will be used.

In experiments carried out so far, we have observed a considerable amount
of iron introduced into the powder while ball milling in a steel jar.  In the case
of GaAs this iron can be leached out, as GaAs dissolves relatively slowly in
HCl.  This operation can not, however, be performed in the case of CdTe which

---

[*]  II-VI Incorporated, Glenshaw, Pa.

13

dissolves rapidly in HCl.

There is evidence that the steel introduced into the powder comes mostly from wearing of the jar rather than the balls. Hence it is possible to avoid this contamination by using a polyethylene bottle as a jar while milling the CdTe crystals.

While admittedly, current procedures are not conducive to high purity in the case of CdTe, a high purity process of general applicability to III-V and II-VI compounds is being explored. In this method, small crystals ( of submicron size range ) are grown by condensation from vapor phase, in an evaporator which is filled to a pressure of a few tenths of a torr with purified inert gas. With this residual pressure in the system, atoms of semiconductor in the vapor phase have a small mean free path. They collide with inert gas atoms, thereby losing energy and condensing in the cold parts of the evaporator. These condensed atoms will serve as nuclei for the growth of small crystals. Any resulting agglomerate with loosely adhering particles can be readily broken up by ultrasonic vibration.

## c. 1. Mechanical Behavior of III-V and II-VI Compounds

S. M. Copley and V. Swaminathan

The objective of this investigation is an understanding of the mechanical behavior of various candidate window materials. Such an understanding is needed because:

(1) The window is a load-bearing structure which is subjected to static and aerodynamic loads.

(2) Thermomechanical techniques are a promising approach for window fabrication.

In previous reports we have described the results of stress-strain experiments on single crystals of Si-doped GaAs. This work is continuing and an abstract describing it has been submitted to the American Ceramic Society for presentation at the Fall Meeting at Pittsburgh, Pa.. In this report, we shall describe the results of experiments to determine the effect of various thermal and thermomechanical treatments on the microstructure and absorption coefficient of GaAs. We have also investigated the microstructure of several types of GaAs with low absorption coefficients in the as-received condition and the results of this investigation will also be included.

### Characterization of As-Received Material

Transmission electron photomicrographs have been obtained for the high resistivity, undoped GaAs (WA1000) and the Cr-doped GaAs ( Bell and Howell ), both in the as-received condition. The undoped material, Fig. 1a, was observed to have a very low dislocation density ( about one dislocation per foil ). The Cr-doped material, Fig. 1b, had a somewhat higher dislocation density. No precipitates were observed in foils of either material.[*] The dark regions in Fig. 1b are artifacts at the foil surface.

### Thermally Diffuse Scattering[**]

Diffuse intensity streaks have been observed in transmission electron

---

[*] What appeared to be precipitates were observed in the first foils of the Cr-doped material that we examined. We have been unable to reproduce these observations after examining many additional foils prepared from the Cr-doped material.

[**] Work described in this section was carried out in collaboration with Prof. G.H. Narayanan, Dept. of Materials Science, University of Southern California.
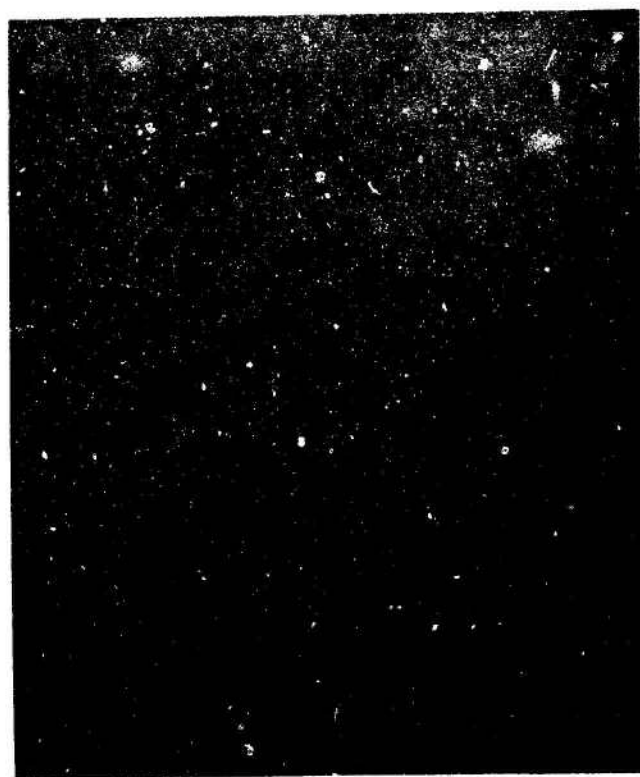
Fig. 1.    As received GaAs single crystals (a) WA-1000 high-resistivity, undoped materials (b) Bell and Howell Cr-doped material
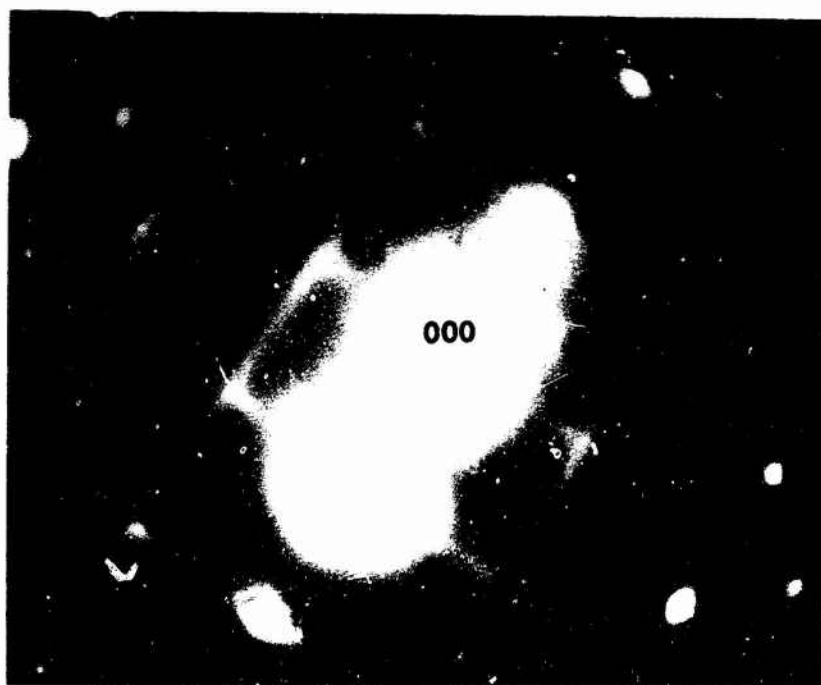
Fig. 2    Diffuse intensity streaks in electron
diffraction pattern of GaAs ( electron
beam approximately parallel to [001] )

diffraction patterns of both undoped and doped GaAs. These streaks, which are shown in Fig. 2, can be regarded as arising due to the intersection of {110} sheets of intensity in reciprocal space with the Ewald sphere. A systematic study of the variation of streak intensity with the crystallographic orientation of the incident beam indicates that these streaks can not be caused by planar defects such as thin platelike precipitates, twins or stacking faults. Futhermore, no indication of rod-like precipitates has been found either in bright field or by dark field imaging of the diffuse streaks. It is believed that the diffuse intensity streaks are of thermal origin similar to diffuse streaks observed in a variety of other materials including Al, Si, Ge, Fe and KCl ( see review paper by Honjo et al[1] ). We have recently found that by hot-stage electron microscopy the intensity of the diffuse streaks increases with increasing temperature thus supporting the hypothesis that the streaks are of thermal origin. A paper describing these observations is in preparation.

## Annealing Treatment

A comparison of the absorption coefficient of the Cr-doped GaAs ( Bell and Howell ) to that of the high-resistivity GaAs (WA-1000), see Section f.1 Fig. 1 , suggests that the difference may be due to absorption by a small volume fraction of precipitates. According to Sparks and Duthler[2], the absorption cross section for a spherical metallic inclusion is given by the equation

$$\sigma_{abs} = 12\ \epsilon_H^{\frac{3}{2}}\ (\frac{\omega}{\omega_p})^2\ \frac{\Gamma a}{c}\ \pi a^2 \tag{1}$$

where

$\epsilon_H$   = dielectric constant of matrix

$\omega$   = frequency of radiation

$\omega_p$   = plasma frequency

$\Gamma$   = relaxation frequency

$c$   = velocity of light

$a$   = radius of the inclusion

The contribution of the inclusions to the absorption is

$$\Delta\beta = \sigma_{abs} N_I \tag{2}$$

where $N_I$ is the number of inclusions per unit volume. Setting $\epsilon_H = 12$,

18

diffraction patterns of both undoped and doped GaAs. These streaks, which are shown in Fig. 2, can be regarded as arising due to the intersection of {110} sheets of intensity in reciprocal space with the Ewald sphere. A systematic study of the variation of streak intensity with the crystallographic orientation of the incident beam indicates that these streaks can not be caused by planar defects such as thin platelike precipitates, twins or stacking faults. Futhermore, no indication of rod-like precipitates has been found either in bright field or by dark field imaging of the diffuse streaks. It is believed that the diffuse intensity streaks are of thermal origin similar to diffuse streaks observed in a variety of other materials including Al, Si, Ge, Fe and KCl ( see review paper by Honjo et al[1] ). We have recently found that by hot-stage electron microscopy the intensity of the diffuse streaks increases with increasing temperature thus supporting the hypothesis that the streaks are of thermal origin. A paper describing these observations is in preparation.

## Annealing Treatment

A comparison of the absorption coefficient of the Cr-doped GaAs ( Bell and Howell ) to that of the high-resistivity GaAs (WA-1000), see Section f.1 Fig. 1 , suggests that the difference may be due to absorption by a small volume . ction of precipitates. According to Sparks and Duthler[2], the absorption cross section for a spherical metallic inclusion is given by the equation

$$\sigma_{abs} = 12 \ \epsilon_H^{\frac{3}{2}} \left( \frac{\omega}{\omega_p} \right)^2 \frac{\Gamma a}{c} \ \pi a^2 \tag{1}$$

where

$\epsilon_H$ = dielectric constant of matrix

$\omega$ = frequency of radiation

$\omega_p$ = plasma frequency

$\Gamma$ = relaxation frequency

$c$ = velocity of light

$a$ = radius of the inclusion

The contribution of the inclusions to the absorption is

$$\Delta \beta = \sigma_{abs} N_I \tag{2}$$

where $N_I$ is the number of inclusions per unit volume. Setting $\epsilon_H = 12$,
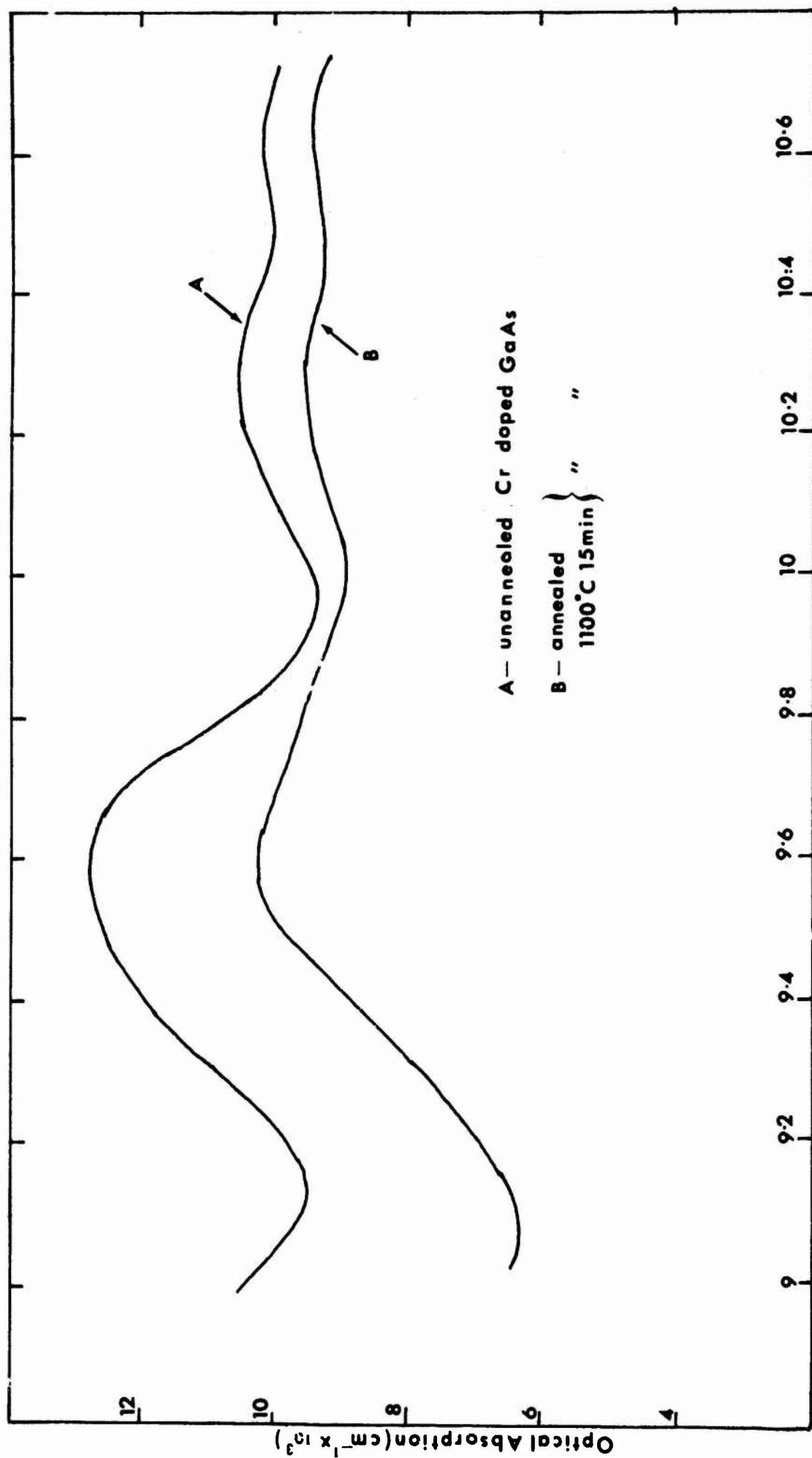
18

Fig. 3 Optical absorption versus wavelength curve for unannealed and annealed Cr-doped GaAs

A — unannealed Cr doped GaAs

B — annealed 1100°C 15min $\left.\right\}$ " "

Optical Absorption (cm$^{-1}$ x 10$^3$)

Wavelength $\mu$

19

$\omega_p = 5 \times 10^{15}$ sec$^{-1}$, $\Gamma = 10^{13}$ sec$^{-1}$ and a $= 100$ Å , we obtain $\sigma_{abs} = 7.6$ Å$^2$ for radiation with a wavelength of 10.6 $\mu$. Setting $\beta = 1.2 \times 10^{-3}$ cm$^{-1}$, see Section f.1 , Fig. 1 , we obtain $N_I = 1.58 \times 10^{12}$ cm$^{-3}$. Since the volume of material shown in a typical photomicrograph is 1 $\mu \times$ 1 $\mu \times$ 0.1 $\mu = 10^{-13}$ cm, the number of particles contained in such a volume for the observed $\Delta\beta$ is 0.158 ( i.e., one inclusion should be observed in seven such volumes ). If the absorption is caused by larger inclusions, they should have a lower density. Thus, if the absorption difference between the Cr-doped and undoped materials at 10.6 $\mu$ is due to inclusions, these inclusions might have escaped detection due to our limited number of observations. It should be noted that the increase in the absorption difference between the Cr-doped and undoped materials with decreasing wavelength is consistent with inclusion absorption according to Eqns (1) and (2).

To further investigate the possibility that inclusions were responsible for the difference in absorption between the Cr-doped and the undoped materials, it was decided to anneal and quench the Cr-doped material. If the difference in absorption was due to inclusions it was reasoned that it might be reduced by a solutionizing anneal. Accordingly, the Cr-doped material was sealed in a silicon tube, annealed at 1100$^{\circ}$C for 15 minutes and then rapidly cooled. A comparison of the absorption coefficients of the annealed and as-received specimens is shown in Fig. 3. The annealing treatment produces a decrease in absorption coefficient and the amount of the decrease becomes greater with decreasing wavelength. The absorption coefficient of the annealed Cr-doped GaAs is comparable to the as-received high resistivity undoped (WA 1000) material.

Figure 4 shows an electron photomicrograph of the annealed Cr-doped material. The most obvious change upon annealing ( see Fig. 1b ) is the reduction in dislocation density.

Cold Working and Process Annealing

Two approaches may be distinguished for fabricating windows by thermo-mechanical means. In the first, called "hot-working", the material is deformed at a temperature that is sufficiently high for recrystallization to occur. This method provides an attractive approach for fabricating windows of the alkali halides due to their strong tendancy to cleave and their lack of five independent
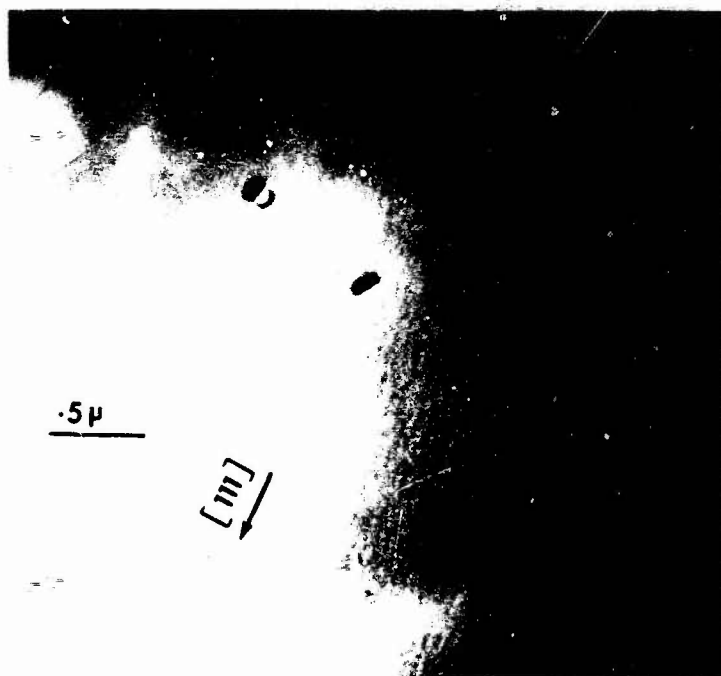
Fig. 4    Bell and Howell Cr-doped GaAs, annealed
          for 15 minutes at 1100°C



Fig. 5    Dislocation substructure of Si-doped GaAs,
          deformed 3 pct at 550°C

21

slip systems. In the second, called " cold-working and process annealing ",
the material is deformed at a temperature too low for recrystallization to occur.
The material is then annealed at a temperature sufficient to effect recrystallization.
This approach is attractive for GaAs because process annealing can be carried
out in a controlled atmosphere to suppress oxidation and arsenic loss. Further-
more, GaAs does not have as strong a tendancy to cleave as the alkali halides
and the primary a/2 $\{111\}<1\bar{1}0>$ slip systems in this material comprise five
independent slip systems. Thus substantial ductility at temperatures below
the recrystallization range is anticipated.

Experiments to explore the possibility of fabricating GaAs windows
by cold working and process annealing have been carried out on Si-doped GaAs.
Although this material is unsuitable for windows, it is believed that its response
to thermomechanical treatments should be the same as materials that are
suitable such as the Cr-doped or the high resistivity undoped GaAs.

Figure 5 shows the dislocation substructure of a Si-doped GaAs crystal
deformed 3 pct at $550^{\circ}$C. One particularly noticable feature is the occurance of
many long straight segments of screw dislocation. Considerably greater strain
than 3 pct is required to produce recrystallization upon subsequent annealing.

Figure 6 shows the dislocation substructure in a Si-doped GaAs crystal
after it was deformed 15 pct at $500^{\circ}$C and annealed in an evacuated and sealed
silica tube at $800^{\circ}$C for one hour. The annealing treatment has caused a
considerable reduction in the density of dislocations. Dislocations have been able
to react during the annealing treatment to produce networks. Another feature
worth noting is the occurance of many small prismatic loops. This structure
is regarded as "recovered" and not "recrystallized" because the lack of
misorientation between regions could be interpreted as grains.

Figure 7 shows the dislocation substructure of a Si-doped GaAs crystal
deformed 20 pct at $550^{\circ}$C and process annealed in an evacuated and sealed silica
tube for 10 minutes at $1100^{\circ}$C. This substructure which is regarded as
recrystallization consists of extensive networks of dislocations bounding regions
that have a significant misorientation with respect to one another. This mis-
orientation is evidenced by the change in contrast upon crossing a dislocation
network which can be seen in Fig. 7.

22

Fig. 6    Recovered structure of Si-doped GaAs deformed
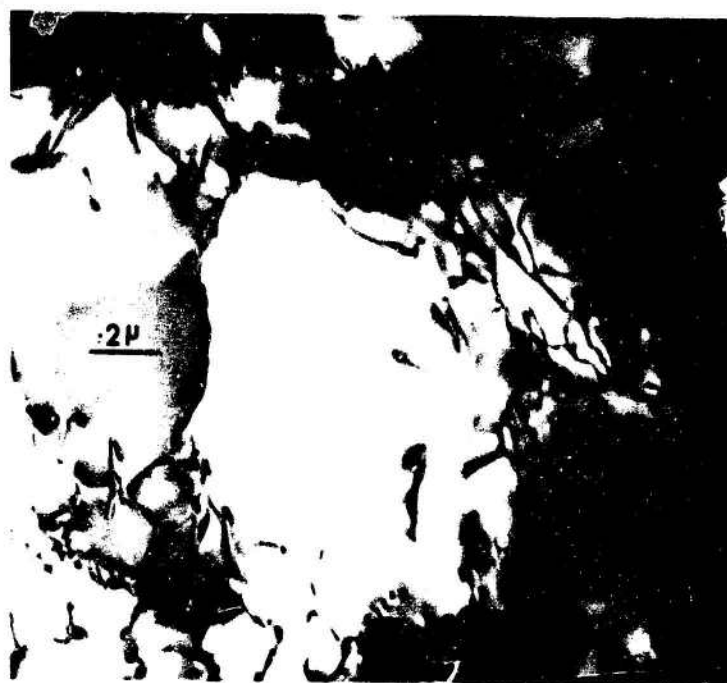15 pct at 500°C and annealed for one hour at 800°C



Fig. 7    Recrystallized structure of Si-doped GaAs, deformed
20 pct at 550°C and annealed for ten minutes at 1100°C

23

All thermomechanical studies to date have been carried out on single crystals. Recrystallization of a initially polycrystalline material by cold working and process annealing would have been somewhat easier because in the recrystallization process grain boundaries are known to be the preferred sites for nucleating new grains. It is believed that recrystallized GaAs may well show improvements in absorption in comparison to melt grown single crystals. This is because the recrystallization process may lead to a redistribution of impurities along grain boundaries.

Cold working and process annealing experiments are continuing and will be extended to the Cr-doped and high resistivity undoped materials. The effect of recrystallization on the absorption coefficient of these materials will be determined.

## References

1. G. Honjo, S. Kodera, and N. Kitamura, " Diffuse Streak Patterns from Single Crystals ", J. Phys. Soc. Japan 19. 351-67 (1964).

2. M. Sparks and C.J. Cuthler, " Theory of Infra-red Absorption and Material Failure on Crystals Containing Inclusions ", Technical Report, Xonics Corp., Van Nuys, Calif. (1973).

## Publications

1. Abstract submitted to 1973 Fall Meeting of the Basic Science Division of the American Ceramic Society, Pittsburgh, Pa. ( Sept. 23-26 ).

   Mechanical Behavior of Si-Doped GaAs Single Crystals

   V. Swaminathan and S. M. Copley

   Stress-strain behavior of single crystals of Si-doped GaAs has been investigated. Stress-strain curves for crystals loaded at a constant stress rate in compression along <100> and <111> have been obtained as a function of temperature at temperatures up to $550^{o}C$. The distribution of dislocations in deformed crystals has been determined by thin-foil transmission electron microscopy. Dislocation mechanisms will be discussed.

2. G.H. Narayanan and S. M. Copley, " Anomalous Diffuse Intensity Streaks in the Electron Diffraction Patterns of GaAs Single Crystals " ( in preparation ).

24

### d. 1 Surface and Interface IR Absorption
### Clarence C. Crowell, T. Mangir

During this quarter we have continued our efforts to build and test the MIS device which is described in detail in previous reports. This device configuration would supply us with information about surface states at the air-GaAs interface. (which is reported to have density of the order of $10^{11} cm^{-2}$ for fast states by Pilkuhn[*]).

To date, we have not been able to observe the variation of MIS capacitance with gate voltage and frequency, and we have not yet obtained desired (~1000 Å) flatness on a large enough sample area (~1 $cm^2$). Because of these results, we have undertaken a closer, more detailed study of the effect of surface preparation.

For this purpose we have examined the surfaces using infrared microscopy, after each stage of preparation. The preparation steps are as follows:

1.  GaAs wafers are degreased 10 min. in warm TCE and 10 min. in boiling Methanol, then etched in a 1 $H_2O_2$: 3 $H_2SO_4$: 1 $H_2O$ solution for 6-7 minutes. Figure 1 shows the wafer at this stage.

    This step removes most of the saw damage.
2.  The wafers are then mounted on a polishing block and polished with Microlite for about 1 hr.

3.  They are then rinsed with neutralizing soap and DI water.

4.  Finally, the samples are etched in 1 $H_2O_2$: 3 $H_2SO_4$: 1 $H_2O$ 1½ min.

Steps 2 to 4 are repeated to achieve a better flatness. The surface after completing step 3 for the first time appears as in Fig. 2.

Fig. 2: The definite orientation of wires on the surface is due to the saw damaged layer. It is also obvious that there is a differently absorbing region which appears as the brighter dot on the picture.

Fig. 3: It shows the surface after completing step 4 for the first time. Pattern which is due to saw damage has about disappeared.

After repetition of steps 2-4 the surfaces appear to be flat to the order of 3000 Å under multiple beam interferometer.

The appearance of a differently absorbing region in the pictures lead us to suspect the presence of some inclusions, or precipitates or gross crystal defects in the material. Such nonuniformities could cause the flatness problems, because of resulting preferential etching, when they appear on the surface.

Some conducting irregularly shaped objects were observed on the GaAs surfaces with the SEM (cf Fig. 5). This material is nominally doped to $10^{17} cm^{-3}$ and was chosen for the MOS studies. The exact source and nature of the inclusions is not yet clear.

At present we are trying to analyze these "impurities" by a probe technique and get some new material to work with.

REFERENCE:

1.    Pilkuhn, M. H., J. Phys. Chem. Solids 25, 141 (1964).

### Dielectric Constant Measurement

### Clarence R. Crowell, S. Joshi

In the course of this research program it became necessary to know the dielectric constant of GaAs accurately to predict infrared losses. In the literature low frequency values of dielectric constant are quoted ranging from 10.9 to 12.5. The frequency and temperature dependence of dielectric constant of GaAs would also be of interest in characterizing the material as a window material for infrared lasers. For these reasons an experimental study of the dielectric constant of GaAs was undertaken.

A simple way to measure the dielectric constant of an insulator is to measure the dielectric capacitance of the material between two parallel conducting plates which act as electrodes. In a practical semiconductor whose resistivity is finite, the measurement frequency should be high enough to avoid effects due to the dielectric relaxation time associated with free carrier redistribution. Also in order to avoid the effects of deep impurities, the capacitance measuring frequencies should be in excess of that corresponding to the deep level response time. This necessitates that the material be of as high a resistivity and as little compensated as possible. Measurements can be per-

formed at lower temperature at which carrier concentration and deep level response time will be reduced.

Another problem associated with the metal-semiconductor system is the intrinsic potential barrier associated with the metal-semiconductor contact. To ensure that the depletion layers under the contacts extend throughout the sample, the Debye screening length associated with the carriers must be much larger than the sample thickness, i.e. the effective dielectric capacitor thickness must be the thickness of the sample. To further assist in ensuring the above condition one should also use contacts that inject neither holes nor electrons into the GaAs. Typical Schottky barriers on GaAs should satisfy this criterion. A good final check on such data should however be that the final capacitances should be independent of applied dc bias.

Bearing the above criteria in mind a GaAs sample of about $10^8$ ohm-cm resistivity with intrinsic carrier concentration was selected. The sample was lapped to a thickness of about 5 mils. Gold electrodes were then evaporated on both sides of the sample. Preliminary measurements have been performed at room temperature. The sample preparation involved two deposition cycles and one of the contacts appeared ohmic. Consequently the capacitances measured were slightly sensitive to bias.

Further measurements need to be performed on additional samples with rectifying contacts on both sides and if necessary at lower temperature.
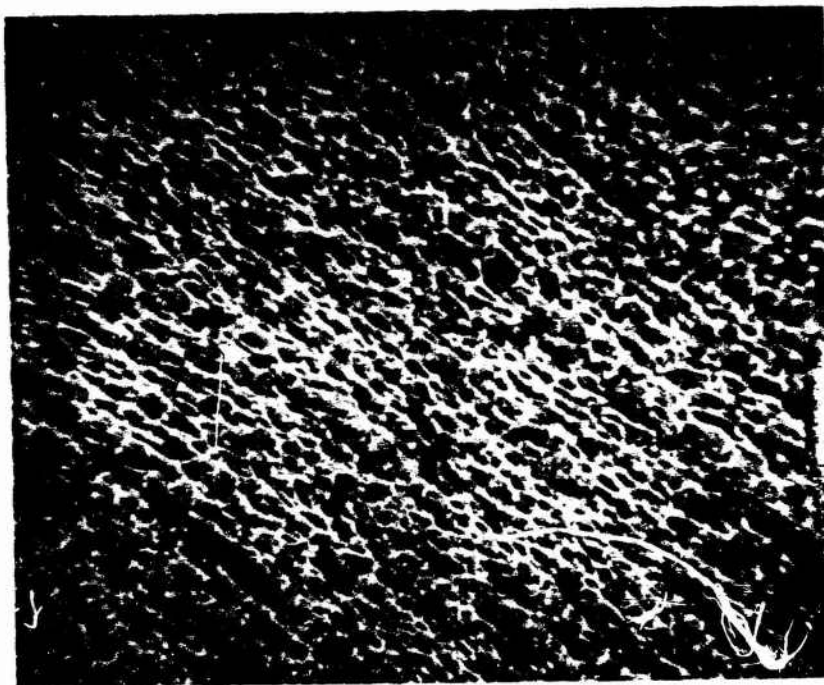
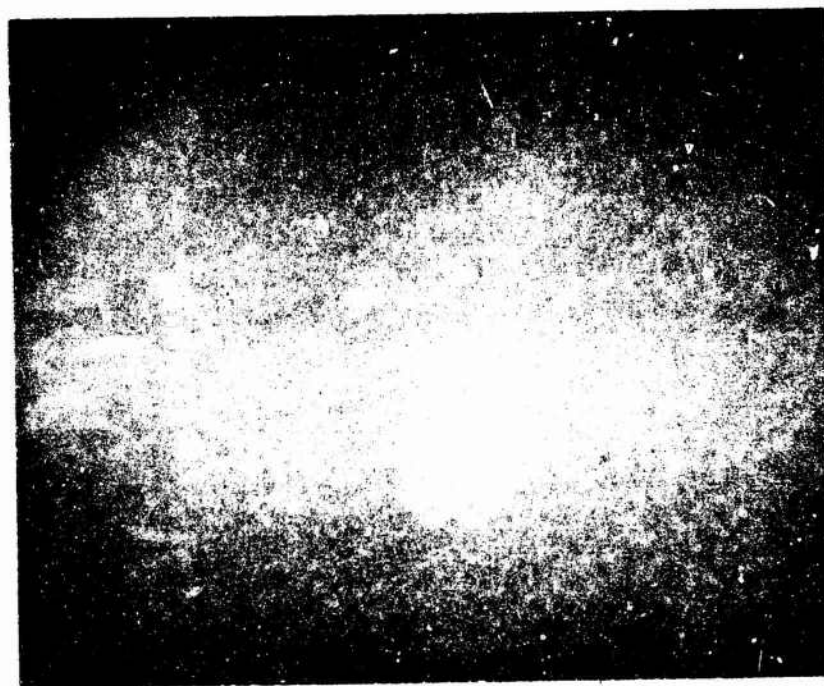Fig. 1  GaAs surface after 1st etching    (10 X)



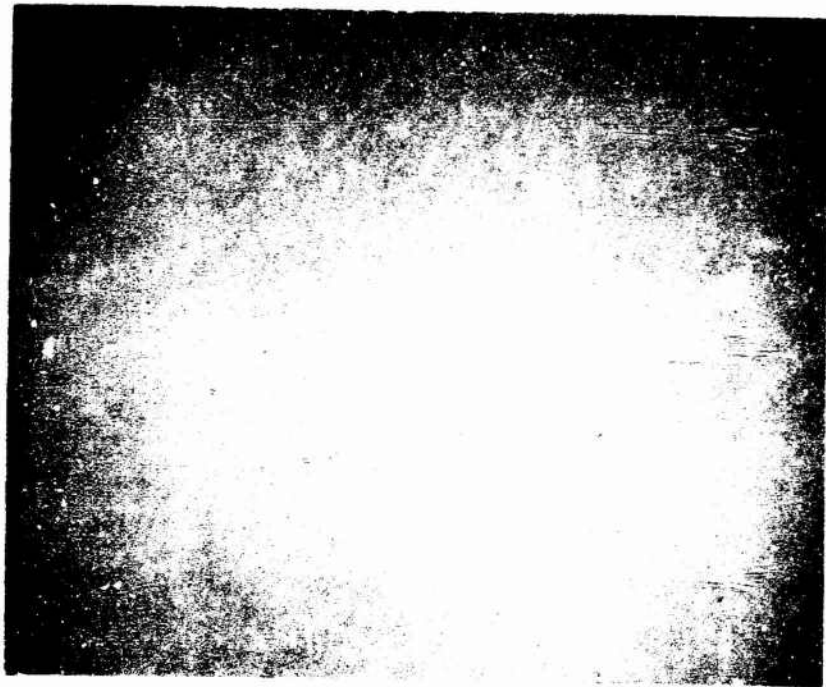Fig. 2:  GaAs surface after step 3 (first time)   (10 X)
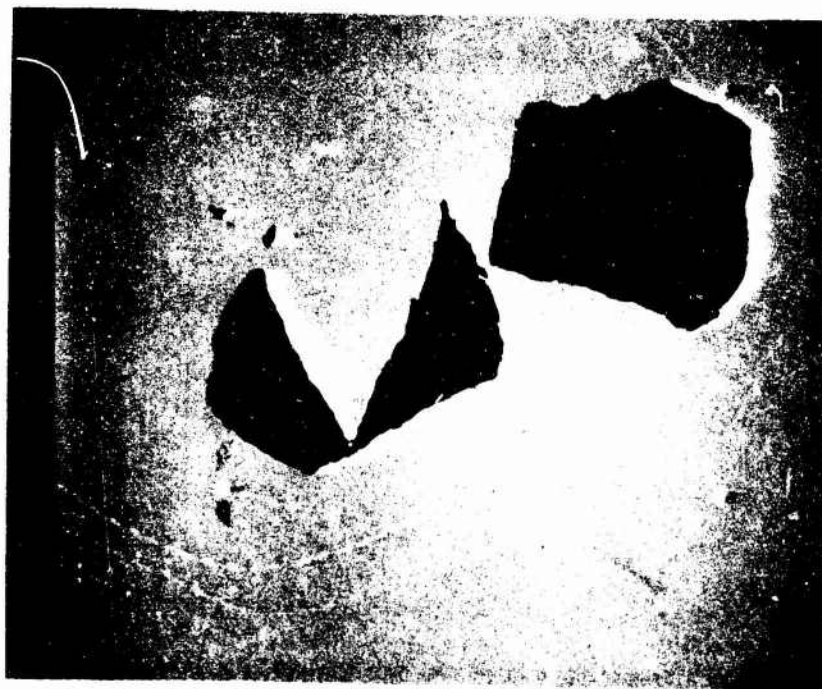
Fig. 3  GaAs Surface after step 4 (1st time)  10 X



Fig. 4  SEM picture of GaAs surface mentioned in text (900X)

29

d. 2   Study of Defects in II-VI Compounds

F. A. Kroger, S. S. Chern, H. R. Vydyanath

1.   Experiments on the self diffusion of Cd in CdTe · In at high indium contents have been completed; a structure in the isotherms indicated by earlier experiments, turns out to be real.

2.   The results are being analyzed in terms of a detailed defect model. Species to be included are:

$V_{Te}^{\cdot\cdot}$ , $Cd_i^{\cdot\cdot}$ , $V_{Cd}''$ , $Te_i'$ , $Te_i^x$ , $In_{Cd}^{\cdot}$ , $In_{Cd}^{\cdot\cdot}$ , $e'$ , $h^{\cdot}$

The introduction of doubly ionized $In_{Cd}$ is necessary to explain an overshoot effect in the Hall effect first tentatively attributed to $In_i^{\cdot\cdot}$. Though In of a higher valency is in general not found, its existence is indicated by compounds such as $In_2Te_5$.

3.   Steps are being taken to get material that allows us to study electrical and optical properties of cooled crystals.

4.   Further study of the function of Ag in CdS has shown that at all Cd pressures, low concentrations of Ag act as donor; at low $p_{Cd}$ higher ones act as acceptors, the electron concentration concentration as $f([Ag])$ passing through a maximum.

At still higher concentration, the Fermi level stabilizes approximately at the level expected in undoped CdS.

e. 1    Theoretical Studies of Absorption Mechanisms in IR Window Materials
        R. W. Hellwarth and M. Mangir

e.1.a   Checks of Multi-phonon Absorption Theory

During this quarter we carried out calculations of weighted averages
over frequency (or'moments') of the multi-phonon absorption in a rocksalt
structure crystal.  All previous calculations of multi-phonon absorption at a
given frequency have required drastic approximations of unknown error.  Our
'moment' calculations however are exact to a given order in the anharmonicity
parameter, and have printed out several types of errors in existing multi-
phonon absorption theory.  For example, we have found       a) that absorption
of a photon leading to the production of an even number of phonons should vanish
in the limit of very unequal ionic masses, and  b) the actual temperature depend-
ence of a given moment is different than that which would have been predicted for
the same interaction potential by previous theories.  The details of this work
and its results are set forth in the accompanying Appendix.  We believe  the
calcu.ation of moments will develop into a valuable tool for understanding multi-
phonon absorption.


e.1.b   Linear and Nonlinear Electric Moments

This quarter we continued the search for practical experimental methods
for determining whether or not, in a given window material, multi-phonon ab-
sorption is mediated mainly or in part by a nonlinear relation between the macro-
scopic electric moment per unit volume (i.e., polarization density) and the local
ionic displacements.  No clearly practical methods have yet been found,  and
the search continues.  In this regard we are collaborating with Dr. Crowell on
this project on the interpretation and re-determination of the dc dielectric
constant of GaAs and other window materials.  There is great disagreement on
this quantity in the literature and it does reflect the presence or absence of a
nonlinear moment.

e.1.c   Multi-Phonon Absorption Calculations

In the second quarterly report of this project we gave numerical results
for the multi-step absorption of a slightly anharmonic diatomic molecule.  A
lattice of these non-interacting molecules was argued to have a 'multi-phonon'
absorption spectrum which, when smoothed,  should resemble that of a real

lattice of interacting units cells. In fact we found that a degree of molecular anharmonicity which was consonant with that known to exist from bulk modulus and other data reproduced well the exponential fall-off with frequency of the wing absorption that has been documented experimentally by Deutsch. At the time we noticed a curiousity of the anharmonic molecule absorption which, for the record, we reproduce below.

When the exact vibrational line spectrum of such a molecule is plotted, unsmoothed, the locus of the line peaks gives a startingly realistic plot of a typical alkali halide absorption spectrum, from an asymmetrically broadened fundamental absorption band to the subsidiary multi-phonon peaks that are increasingly broadened and washed-out at higher phonon numbers. A typical such molecular absorption spectrum is shown in figure 1 with the molecular parameters adjusted to fit the measured wing abosrption of KCl crystal at 300K. That the resemblance of this to a crystal spectrum should exist when the ionic masses are very different is printed out in Appendix I. (In this case each light ion essentially vibrates independently in a rigid cage of heavy ions). However, we have no proof that the resemblence is more than accidental for a crystal like KCl whose masses are close.

KCl

$T = 300°K$

$x = 0.011$
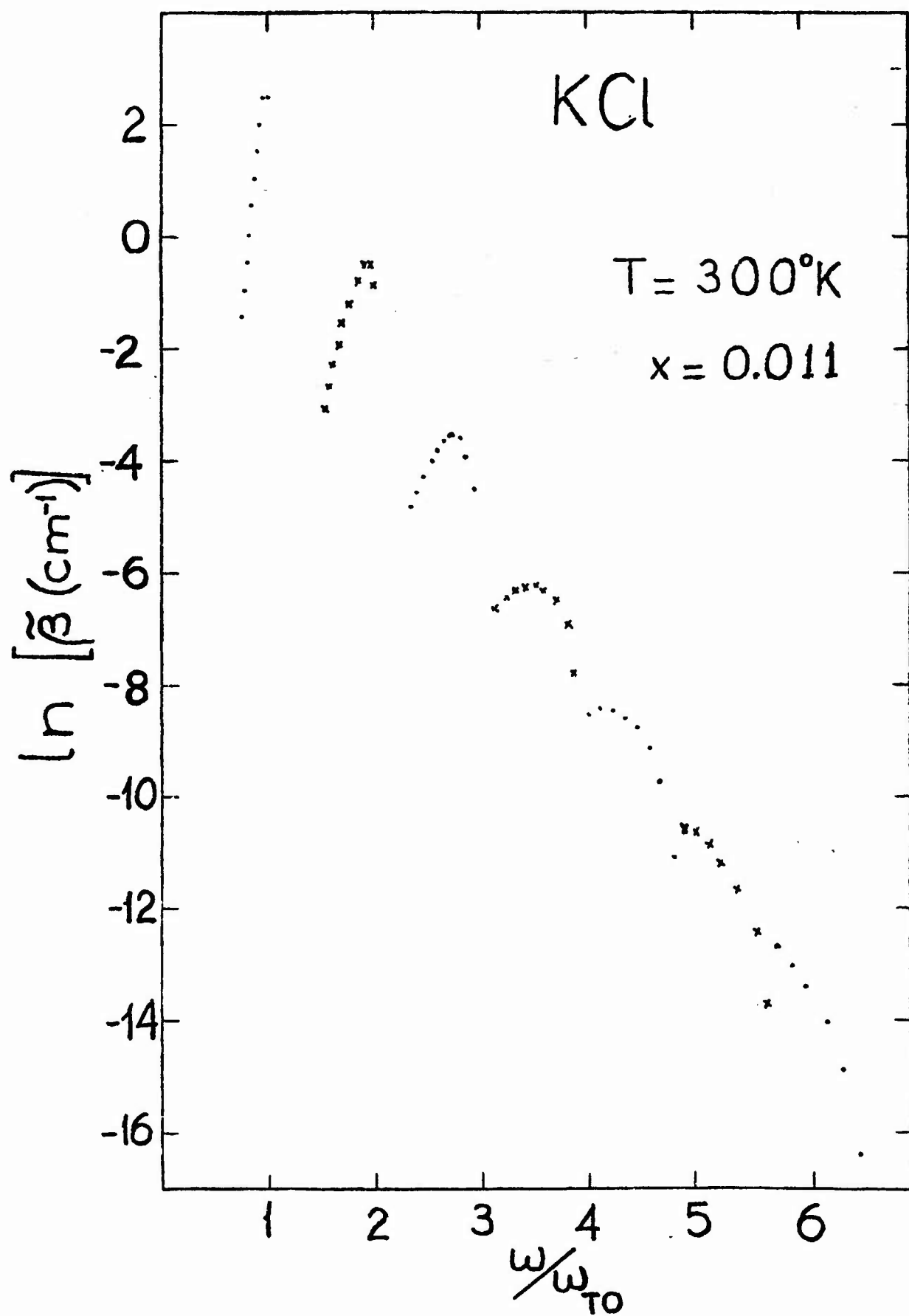
## Caption for Figure 1

Fig. 1. A plot of the line spectrum of a diatomic molecule interacting via a Morse potential with anharmonicity parameter $\underset{\sim}{\chi}$, resonant frequency $\omega_{TO}$, and dipole matrix element adjusted so that $\beta$ from $\omega = 2\omega_{TO}$ to $5\omega_{TO}$ is nearly the measured absorption coefficient of a KCl crystal at 300 K. The modified absorption coefficient $\widetilde{\beta}$ is defined as $4\pi N a''(\omega)/nc$ where $a''$ is the imaginary part of the molecular polarizability at $\omega$, N is the number density of KCl, and N is the refractive index of KCl.

Appendix for e.1

Checks of Multi-Phonon Absorption Theory[*]

Robert Hellwarth

Departments of Electrical Engineering and Physics
University of Southern California
University Park
Los Angeles, California   90007

There is considerable uncertainty as to the accuracy of calculations to date of multi-phonon absorption in infrared window materials.   Here we show that such uncertainties can be checked by calculating various weighted integrals over frequency ("frequency moments") of the imaginary part $\chi''(\omega)$ of the electrical susceptibility, to which the absorption coefficient $\beta(\omega)$ cm$^{-1}$ is related.   We obtain expressions for six moments, evaluating a moment of the 2-phonon contribution explicitly for an anharmonic pair-interaction model.   This exact result reveals inaccuracies in the dependence of absorption on ion masses and temperature predicted by approximate theories.

Key Words:  Crystal absorption theory, frequency moments, infrared absorption, infrared susceptibility, infrared window materials, multi-phonon absorption.

## I.   Introduction

There has been a number of theoretical efforts to estimate the intrinsic infrared (IR) absorption coefficient $\beta(\omega)$cm$^{-1}$ of IR window materials in the high-frequency "tail" of the fundamental lattice absorption.[1-7][1]   This absorption is presumably "multi-phonon"; that is, an absorbed photon is converted to m-phonons so as to conserve energy and crystal momentum, and obey certain selection rules.[8,9]   Numerical predictions from the m-phonon theories for $\beta$ have had to rely on rather drastic approximations that leave uncertain the magnitude of the theoretical errors.[1-7]   Here we point out that various weighted integrals over frequency of the imaginary part $\chi''(\omega)$ the lattice electric susceptibility can be evaluated exactly, or at least to known accuracy.   Since $\chi''$ is related to $\beta$, the predicted values of these "moments" can be used to check the accuracy of the theories of $\beta$.   We perform such a check of 2-phonon absorption in a diatomic cubic crystal, and point out errors in existing theoretical results for the mass and temperature dependence of this absorption.   For example, we find that a)  this absorption should be small when the ionic masses are very different, and b)  when the masses are equal, the variation of the 2-phonon absorption, in going from low to high temperatures, is really about twice that predicted by previous approximate theories.

In Section 2, we review the quantum expressions for $\beta$ and $\chi$ (the electric susceptibility). In Section 3, we define the moments of $\chi(\omega)$ and obtain the quantum formulae for six of them, in terms of averages over various derivatives of the interionic potential, assuming a linear relation to exist between the dipole moment operator and the ionic displacements (i.e., a "linear dipole moment").   We derive as an example in Section 4 the fifth frequency moment of the 2-phonon absorption for an anharmonic pair potential. Then in 5, we compare our predicted mass and temperature dependence with that from the approximate theories of $\beta$.

---

[1] Figures in brackets indicate the literature references at the end of this paper.

## 2. Quantum Theory of Absorption and Susceptibility

At optical frequencies well below the bandgap, we may picture a window material as composed of ions (labelled by greek indices $\alpha, \beta, \ldots$) having masses $m_\alpha$, and interacting via a potential V that is a function of their position vectors $r_\alpha$. The electronic interactions are absorbed in the ion dynamics via the Born-Oppenheimer approximation. This gives an effective Hamiltonian H for a subvolume $L^3$ of the material (where L is much less than an optical wavelength but much greater than the interionic spacing) of the form

$$H = \tfrac{1}{2}\Sigma_{i,\alpha} p_{i\alpha}{}^2/m_\alpha + V \tag{1}$$

where the $p_{i,\alpha}$ are the components ($i=x,y,z$) of the momentum operator for the ion $\alpha$. The potential V does not include long range interactions between ions in $L^3$ and in neighboring regions. These interactions are assumed to be mediated by the long wavelength components of the electric field $\vec{E}$, that is, by the macroscopic electric field, the transverse part of which is the propagating field whose absorption coefficient we seek. The field interacts with the subvolume $L^3$ via a perturbation $-ME-\tfrac{1}{2}\chi_e E^2$ where $\chi_e$ is the electronic susceptibility with ions fixed, and M, the component of the electric dipole moment in $L^3$ along $\vec{E}$, is taken to be

$$M = \Sigma_\alpha e_\alpha x_\alpha \tag{2}$$

where $e_\alpha$ is effective charge of the ion $\alpha$, and $x_\alpha$ is the component of the displacement from equilibrium of ion $\alpha$ along the direction of $\vec{E}$. We neglect here the terms in M that are not linear in the $x_\alpha$ as this is thought to be accurate for most polar insulating materials and has been assumed in most theories of multi-phonon absorption.

The complex/electric susceptibility $\chi_i$ at frequency $\omega$ of an optically isotropic crystal is defined as

$$\chi_i(\omega) = L^{-3} <M(\omega)>/E(\omega) \tag{3}$$

Where $<M(\omega)>$ is the expected amplitude of the electric moment in $L^3$ oscillating in response to the macroscopic field of amplitude $E(\omega)$. The absorption coefficient is related to $\chi = \chi_e + \chi_i$ by

$$\beta(\omega) = \frac{2\omega}{c} \text{ Im } [1 + 4\pi \chi(\omega)]^{\frac{1}{2}} \tag{4a}$$

$$\rightarrow \frac{4\pi \chi''(\omega)\omega}{nc}, \quad \chi'' << 1. \tag{4b}$$

Here $\chi''$ is the imaginary part of $\chi_i$, c is the velocity of light in a vacuum and n the refractive index. We now write the well-known quantum mechanical formula for $\chi''$ in terms of the ion-ion response functions $S_{\alpha\beta}(\omega)$ for which we will derive simple moment formulae:

$$\chi''(\omega) = \pi L^{-3} \Sigma_{\alpha,\beta} S_{\alpha\beta}(\omega) e_\alpha e_\beta \tag{5}$$

where

$$S_{\alpha\beta}(\omega) \equiv \Sigma_{m,n}(P_m - P_n)<m|x_\alpha|n><n|x_\beta|m>$$
$$\cdot \delta(\omega-\omega_{nm})/(2\hbar) + (\alpha \rightleftarrows \beta). \tag{6}$$

Here $|m>$ is an eigenstate of the Hamiltonian H for the subvolume $L^3$ having energy $E_m$ and probability $P_m$ of occupation. $\hbar\omega_{nm} = E_n - E_m$. It is from this exact formulation (5) and (6) for $\chi''$ that previous theories of $\beta(\omega)$ have started. We proceed instead to derive from (6) formulae for moments of $S_{\alpha\beta}$ and thereby for $\chi''$.

## 3. Moments of Ion-Ion Response Functions

The $\ell^{th}$ moment $S_{\alpha\beta}{}^{(\ell)}$ of the ion-ion response function $S_{\alpha\beta}(\omega)$, as defined by

$$S_{\alpha\beta}(\ell) = \begin{cases} \int_{-\infty}^{\infty} d\omega\,\omega^\ell S_{\alpha\beta}(\omega), & \ell \text{ odd} \tag{7a} \\[2mm] \int_{-\infty}^{\infty} d\omega\,\omega^\ell \coth(\frac{\hbar\omega}{2kT}) S_{\alpha\beta}(\omega), & \ell \text{ even}, \tag{7b} \end{cases}$$

is seen from (6) to equal

$$\hbar^{-\ell-1}\Sigma_{m,n}P_m(E_n - E_m)^\ell <m|x_\alpha|n><n|x_\beta|m> + (\alpha \rightarrow \beta) \tag{8}$$

for thermal equilibrium when $P_n/P_m = \exp(E_m - E_n)/kT$. From (8) it follows directly that

$$S_{\alpha\beta}{}^{(0)} = 2<x_\alpha x_\beta>/\hbar \tag{9}$$

$$S_{\alpha\beta}{}^{(1)} = \delta_{\alpha\beta}/m_\alpha \quad \text{(Thomas-Kuhn-Reich sum rule)} \tag{10}$$

$$S_{\alpha\beta}^{(2)} = \langle x_\alpha (\partial V/\partial x_\beta)\rangle/(m_\beta \hbar) \tag{11}$$

$$S_{\alpha\beta}^{(3)} = \langle \partial^2 V/\partial x_\alpha \partial x_\beta\rangle/m_\alpha m_\beta \tag{12}$$

$$S_{\alpha\beta}^{(4)} = 2\langle (\partial V/\partial x_\alpha)(\partial V/\partial x_\beta)\rangle/m_\alpha m_\beta \hbar \tag{13}$$

$$S_{\alpha\beta}^{(5)} = \Sigma_{\alpha,i} \langle (\partial^2 V/\partial x_\alpha \partial r_{i\alpha})(\partial^2 V/\partial x_\beta \partial r_{i\alpha})\rangle/m_\alpha m_\beta m_\alpha \tag{14}$$

by repeated use of the identity

$$(E_m - E_n)\langle m|A|n\rangle = \langle m|[H,A]|n\rangle \tag{15}$$

where A is any operator and H is the Hamiltonian operator of (1). In (14), $r_{i\alpha}$ is the displacement of ion $\alpha$ in a direction i=x,y,z. In (9) - (14) the $x_\alpha$ are displacements parallel to the applied electric field.

### 4. Application to Pair Interactions With Hard Cores

The interaction potential V of ionic crystals is known to be fairly well represented by a superposition of pair potentials

$$V \rightarrow \tfrac{1}{2}\Sigma_{\alpha,\beta} v(\vec{x}_\alpha - \vec{x}_\beta + \vec{R}_\alpha - \vec{R}_\beta) \tag{16}$$

where $\vec{x}_\alpha$ is the displacement from equilibrium position $\vec{R}_\alpha$ of ion $\alpha$. In multi-phonon absorption calculations, the potential V has been assumed to be made up of a harmonic part $V_h$, quadratic in the ion coordinates, and an anharmonic part $V_{an}$, which arises from the hard-core repulsion between nearest neighbors, and which has been assumed to be a power series

$$V_{an} = \Sigma_{\alpha,\beta}\, \Sigma_{r=3}^{\infty} c_n r_{\alpha\beta}^{\,n}/n! \tag{17}$$

in the relative ionic displacement $r_{\alpha\beta}$ along the equilibrium separation vector $\vec{R}_\alpha - \vec{R}_\beta$. ($\alpha$ and $\beta$ are summed over all nearest neighbor pairs.) Since the repulsive part of $v(r)$ is thought to be roughly of the form $\exp{-r/\rho}$, the coefficients $c_n$ are thought to be all of the same order of magnitude, and of the order of a dimensionless anharmonicity parameter $\lambda$ [10]:

$$c_n \sim \lambda \tag{18}$$

where

$$\lambda \equiv \left(\frac{\hbar}{2\omega_0 \mu \rho^2}\right)^{\frac{1}{2}}, \tag{19}$$

$\mu$ is the reduced mass of an ion pair, and $\omega_0$ is the transverse optical (or reststrahl) frequency. The values of $\rho$ for alkali halide crystals have been determined from bulk modulus data and yield values of $\lambda$ around 0.3.

Given some natural assumption about the exact values of $c_n$ (e.g., $c_n = \lambda \times$ constant), the present theories for the absorption $\beta$ are not able to proceed with known accuracy even to calculate two-phonon absorption; the k-space integrals are too complicated. However, we can proceed to find the moments (9)-(14) to some desired order in the anharmonicity parameter. We illustrate this here by finding the part of the fifth moment that is of order $\lambda^2$ and represents multi-phonon absorption.

An examination of $S^{(5)}$ in (14) shows that the only $\lambda^2$ terms are those proportional to $c_2 c_4$ or $c_3^2$. (Here we have used $c_2$ to symbolize the harmonic force coefficients in analogy with the anharmonic coefficients $c_n$ for n>2 in (17).) An examination of the structure of perturbation theory shows that to order $\lambda^2$, the $c_2 c_4$ term describes a shift and broadening of the one-phonon absorption while the corresponding $c_3^2$ term gives rise only to multi-phonon absorption. In fact it describes the rate of all combinations of two-phonon absorption and emission among all phonon branches. This is evident because $c_3$ is the coefficient of all products of three phonon creation and annihilation operators in the perturbing potential, and therefore in the $c_3^2$ term in $\chi''$. These terms contribute a factor to the absorption matrix element that describes the annihilation of the k=0, TO phonon (created by a photon) along with the annihilation or creation (in any combination) of two other phonons from any branches. We now calculate this "2-phonon" contribution $S_{2ph}^{(5)}$ to the fifth moment $S^{(5)}$ of $\chi''$.

Inserting the n=3 term of (17) into (14), performing the indicated differentation, and summing over ions as indicated in (5) gives for a rocksalt structure crystal

$$S_{2ph}^{(5)} \equiv \int_0^\infty d\omega\, \omega^5 \chi''(\omega)_{2\text{-phon}} = \pi c_3^2 e^2 \mu^{-3} L^{-3} \sum_\alpha [\tfrac{1}{2} < (x_\alpha - x_{\alpha-1})^2 >$$
$$- < (x_{\alpha-1} - x_\alpha)(x_{\alpha+1} - x_\alpha) > \mu / m_\alpha ]. \tag{20}$$

Here, $x_{\alpha \pm 1}$ are the relative x-displacements of the nearest neighbors to ion $\alpha$ in opposite directions along the crystal x-axis; e is the magnitude of the effective charges $e_\alpha$ and $e_\beta$, and $\mu$ is the reduced ion pair mass. The thermal averages indicated by $< >$ are needed here only in the harmonic approximation ($\lambda = 0$). For a diatomic crystal, harmonic-crystal quantum theory gives [10]

$$<x_\alpha x_\beta>_{\text{harm}} = \Sigma_Q \frac{\hbar U^{-1}(x, \alpha; Q) U(x, \beta; Q)}{2\omega_Q \sqrt{m_\alpha m_\beta}} \coth \frac{\hbar \omega_Q}{2kT} \tag{21}$$

where the Q labels all the normal modes of the crystal in volume $L^3$, and $\omega_Q$ are their frequencies. The unitary U-matrices are those which diagonalize the matrix $v_{xy,\alpha\beta}(m_\alpha m_\beta)^{-\frac{1}{2}}$ deriving from the expression

$$V_h = \tfrac{1}{2}\Sigma_{xy,\alpha\beta} x_\alpha y_\beta v_{xy,\alpha\beta} \tag{22}$$

for the harmonic part of the potential.

## 5. Comparison With Absorption Theory

There exists no explicit calculation of all 2-phonon processes for a real lattice with an explicit $V_h$ with which we might compare the results (20) and (21) directly. However, we can obtain some interesting checks of absorption theory by examining two extreme rocksalt structure models in which there are either 1) very unequal ion masses, or 2) equal masses and nearest neighbor interactions.

### 5.1  $m_{\alpha+1} \gg m_\alpha$

When the masses of the ions in a rocksalt cubic crystal are very different, then the light ions ($\alpha$) move in a nearly rigid cage of the surrounding heavy ions, making $x_{\alpha+1} - x_\alpha \approx x_{\alpha-1} - x_\alpha$. This with the limit $m_\alpha \to \mu$ causes the two averages in (18) to cancel exactly, indicating that 2-phonon absorption vanishes when $m_{\alpha+1} \gg m_\alpha$. This is reasonable, because the light ion is moving effectively in a potential having inversion symmetry, and its states have even or odd parity. Since dipole transitions are not allowed between states of the same parity, no even number phonon absorption processes will exist in this limit. No hint of this depression of the even-phonon number absorption is found in present approximate theories, although the effect can be seen in the relative experimental heights of the 2-phonon resonance peaks in different alkali halides.[11] This failure probably signals factors-of-two errors in the high-frequency tail absorption of crystals like LiF whose ionic masses are quite different.

### 5.2  $m_\alpha = m_{\alpha+1} = 2\mu$ and Nearest Neighbor Forces Only

When both ion masses are equal and the harmonic forces are between nearest neighbors in a cubic diatomic crystal, the normal lattice modes consist of three degenerate branches whose ion motions are polarized along x, y and z. Since we need only correlations between x-displacements in (20), the sum in (21) is over one branch only. The normal mode coordinates for this branch, as embodied in the unitary U-matrices, are the familiar plane waves

$$U(x, \alpha; Q) = (\tfrac{a}{L})^{\frac{3}{2}} \exp i \frac{2\pi a}{L} (Q_x \alpha_x + Q_y \alpha_y + Q_z \alpha_z) \tag{23}$$

where the modes are labelled by the integers $Q_x, Q_y, Q_z = 0, \pm 1, \ldots \pm \frac{L}{2a}$ and the ions by the integer coordinates $\alpha_x, \alpha_y, \alpha_z = 1, 2, \ldots L/a$. The length of the cube edge of the crystal sub-volume is L and the interionic spacing is a. Diagonalizing the harmonic potential with (23) gives the eigenvalues of the potential matrix and the dispersion relation for the x-branch:

$$\omega_Q = \omega_0 \sin(\pi Q_x a / L), \tag{24}$$

where

$$\omega_0 = (2C/\mu)^{\frac{1}{2}} \tag{25}$$

is the "TO" or fundamental (k=0) optical phonon absorption frequency for the rocksalt structure lattice with equal masses (m=2$\mu$) and nearest-neighbor force constant C.

**Substituting** (23) and (24) in (21) gives for the 2-phonon absorption moment of (20)

$$S_{2ph}^{(5)} = \frac{2c_3^2 e^2 \hbar}{\mu^4 a^3 \omega_o} I(\gamma) \tag{26}$$

where

$$I(\gamma) \equiv \int_0^1 du \; u(1-u^2)^{\frac{1}{2}} \coth \gamma u. \tag{27}$$

The **temperature** parameter $\gamma$ is

$$\gamma \equiv \frac{\hbar \omega_o}{2kT} . \tag{28}$$

**At high temperatures**

$$I(\gamma) \to \frac{\pi}{4\gamma}, \quad \gamma \to 0 \tag{29}$$

and at **low** temperatures

$$I(\gamma) \to \frac{1}{3}, \quad \gamma \to \infty . \tag{30}$$

For **fixed** $\omega_o, \overline{c_3}, e,$ and a, the independent-anharmonic-molecule models [1-4] predicted for this, or any **other** type of lattice, a 2-phonon temperature factor $2\bar{n} + 1$, where $\bar{n}$ is the Planck function $[e^{2\gamma}-1]^{-1}$. Therefore these very approximate theories predict

$$\frac{S_{2ph}^{(5)}(T=0)}{S_{2ph}^{(5)}(T \to \infty)} = \gamma \tag{31}$$

rather **than** the exact result for this lattice model of $4\gamma/3\pi$ from (29) and (30). A plot of $I(\gamma)$ between its asymptotes is shown in figure 1 together with the $2\bar{n}+1$ function normalized to approach $I(\gamma)$ at high temperatures.

It is well-known that this model having only nearest neighbor forces does not accurately describe any real rocksalt-structure ionic crystals. However, we feel that checking a theory by applying it to this model does give a reasonable estimate of its accuracy for a more realistic model of a crystal. That is, the fact that the ratio (31) from approximate theories of absorption is 2.4 times the exact result for this (albeit poor) model is an indication of the kinds of errors for the moments of $\beta$ that the independent-molecule models may yield in the 2-phonon region. It is also likely that the errors are even larger at higher frequencies (higher phonon numbers).

In summary, we have shown how calculations of frequency moments of the imaginary part $\chi''(\omega)$ of the electric susceptibility can be performed with much greater accuracy than can calculations of $\chi''(\omega)$ itself, and how the moment calculations can be used to check the more detailed calculations of multi-phonon absorption $\beta(\omega)$ as a function of frequency. Many other checks and relations may be derived from the moment expressions (9) to (14) than we have mentioned here.

## 6. References

[1] M. Sparks and L. J. Sham, Sol. State Comm. **11**, 1451 (1972) estimated multi-step absorption in a slightly anharmonic oscillator by considering a subset of perturbation theory terms (or "diagrams"). A linear dependence of electric moment on oscillator displacement (a "linear moment") was assumed.

[2] B. Bendow, Phys. Letters **42A**, 359 (1972) calculated the multi-step absorption in a harmonic oscillator arising from non-linear dependence of the electric moment on the oscillator coordinate (a "non-linear moment")

[3] T. C. McGill, R. W. Hellwarth, M. Mangir and H. Winston, J. Phys. Chem. Solids (to be published) calculated exactly multi-step absorption in slightly anharmonic oscillators with both linear and quadratic electric moments.

[4] B. Bendow, S. C. Ying, and S. Yukon (to be published) have constructed a Green's function formulation of the anharmonic lattice having a nonlinear electric moment, and estimated Debye-Waller factors.

[5] M. Sparks and L. J. Sham, Phys. Rev. (to be published) have estimated multi-phonon absorption from a real lattice, having a linear moment, by neglecting crystal-momentum conservation.

[6] A. A. Maradudin and D. L. Mills (to be published) have found the classical limit of the high frequency absorption of a charged particle moving in a variety of potentials.

[7] H. B. Rosenstock, Bull. Am. Phys. Soc. 18, 674 (1973), has summed the thermal phonon population factors over the modes of KCl to obtain better estimates of the temperature dependence of its multi-phonon absorption than come from single-frequency models.

[8] J. L. Birman (to be published) has examined selection rules for the combinations of phonons that can be created by absorbing a photon.

[9] R. A. Cowley, in "Phonons in Perfect Lattices and in Lattices with Point Imperfections" pp. 170-207 (ed. R. W. H. Stevenson, Plenum Press, N. Y. 1966) reviews multi-phonon perturbation theory and some calculations of specific diagrams and spectral features.

[10] L. van Hove, N. M. Hugenholtz, and L. P. Howland "Quantum Theory of Many Particle Systems" (W. A. Benjamin, N. Y. 1961)

[11] L. Genzel, in "Festkörper Probleme" Vol. VI, p. 32 (ed. O. Madelung, Pergamon Press, Oxford 1967).

## 7. Figures
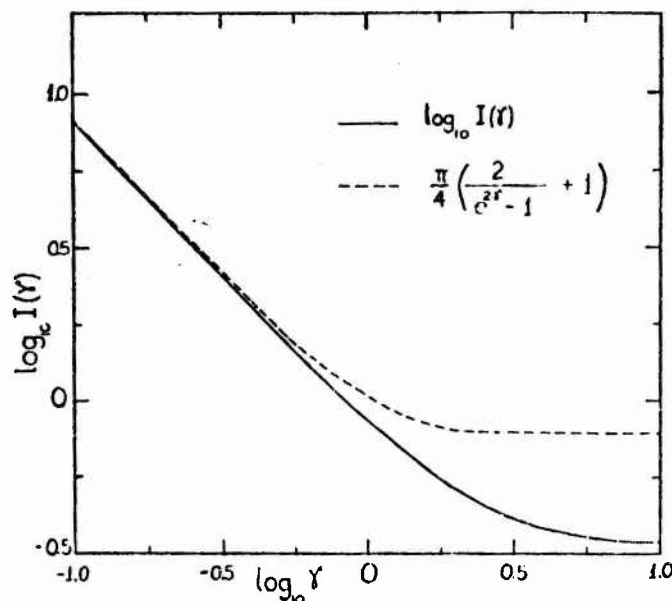


Figure 1. Plot of the temperature factor $I(\gamma)$ calculated for the fifth frequency moment of all 2-phonon contributions to the imaginary part $\chi''$ of the susceptibility of a rocksalt-structure crystal with nearest neighbor interactions. The factor $2\bar{n}+1$ predicted from the independent-molecule approximation for the same moment is shown for comparison, normalized arbitrarily to approach the exact result at high temperatures. $(\gamma = \hbar\omega_o/2kT)$

## f.1 Wavelength Dependent Calorimetry
### W. H. Steier, S. T. K. Nieh, R. Joiner

### NEW SAMPLES

In accordance with our plan of locating the highest purity melt grown GaAs samples grown in the past 5 to 10 years, we have requested and received samples from IBM and Bell Telephone Labs. The IBM samples were prepared by Jerry Woodall using the horizontal bridgeman technique. Before growth oxygen was purposely introduced into the boat and after growth the sample was remelted. (Hence the name WORM-1, With Oxygen ReMelt.) Particular care was given to purity of source material and avoidance of contamination during growth. The result of our calorimetric measurement of WORM-1 is almost identical to that of WA1000 reported in our last quarterly report.

The Bell Telephone Lab's samples were prepared using the float zone technique developed by Professor James Whelan. Table 1 contains information of different samples. Preliminary calorimetric measurements show that the residual optical loss of these samples are similar to that of WA 1000. More detailed measurements are planned to confirm this.

| Sample No. | $\frac{cm^2}{V\ sec}$ Room Temp. Mobility | $\Omega$-cm Resistivity | Comment |
|---|---|---|---|
| 44-3A | 5550 | $4.6 \times 10^8$ | carbon doped |
| 54-4A | 5700 | $2.5 \times 10^8$ | slow pass |
| 55-1A | 6000 | $1.4 \times 10^8$ | slow pass |
| 46-5A | Inhomogeneous | Inhomogeneous | high As pressure |

Table 1 - Bell Telephone Lab Float Zone Samples

## Conclusions

After having measured the highest purity and best crystalline quality melt grown GaAs crystals available anywhere, we are forced to conclude that there is a definite lower limit on the absorption coefficient of about $0.008$ cm$^{-1}$ at $10.6\mu$. The exact nature of the basic mechanism responsible for this loss is not clear at this point. However, we hope to have a better idea after we have obtained the wavelength dependent absorption data as a function of temperature. From the fact that high $\rho$ GaAs needs heavy compensation we can speculate that impurity plays an important role. Localized nonstoichiometry could be another possible mechanism.

Dr. Don Stierwalt of NELC, San Diego recently kindly consented to make emissitivity measurements on a Bell and Howell sample EMC 6012B which has already been measured by us calorimetrically. Figure 1 shows his results with our data superimposed upon it. The emissitivity measurements were made at $373^{\circ}$K and the calorimetry measurements at $300^{\circ}$K. Other measurements near $273^{\circ}$K at NELC are very similar. The agreement between the data is very good and provides an independent check on both measuring techniques. The structure is identical except for a shift in wavelength. This could be a temperature effect, but is probably due to a wavelength calibration error. The USC wavelength calibration is believed to be correct since it agrees with the known output spectra of the $CO_2$ laser. This agreement is a very encouraging result for both the NELC and the USC groups.

## Computer Simulation of Heat Flow in Calorimetry

The two-dimensional heat program TEMPS is now working. An initial run was made using insulated boundary conditions and actual laboratory sample parameters. The computed time rate of change of the surface temperature agreed within 5% with the results obtained from the theory used in the calorimeter measurements.

The three-dimensional heat program HEATING.3 has been received and is being made ready for use.
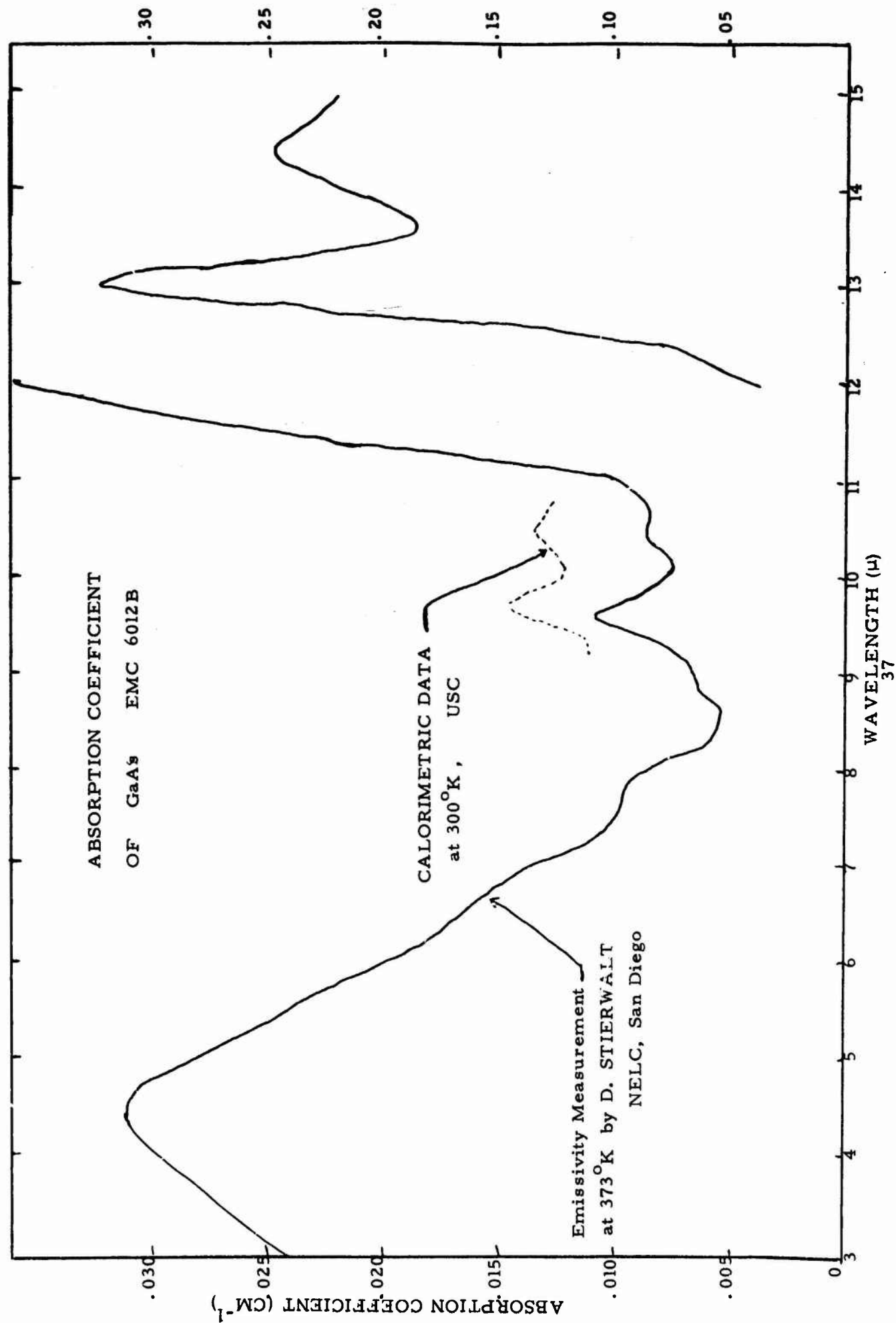
36

## Conclusions

After having measured the highest purity and best crystalline quality melt grown GaAs crystals available anywhere, we are forced to conclude that there is a definite lower limit on the absorption coefficient of about 0.008 cm$^{-1}$ at 10.6μ. The exact nature of the basic mechanism responsible for this loss is not clear at this point. However, we hope to have a better idea after we have obtained the wavelength dependent absorption data as a function of temperature. From the fact that high ρGaAs needs heavy compensation we can speculate that impurity plays an important role. Localized nonstoichiometry could be another possible mechanism.

Dr. Don Stierwalt of NELC, San Diego recently kindly consented to make emissitivity measurements on a Bell and Howell sample EMC 6012B which has already been measured by us calorimetrically. Figure 1 shows his results with our data superimposed upon it. The emissitivity measurements were made at 373°K and the calorimetry measurements at 300°K. Other measurements near 273°K at NELC are very similar. The agreement between the data is very good and provides an independent check on both measuring techniques. The structure is identical except for a shift in wavelength. This could be a temperature effect, but is probably due to a wavelength calibration error. The USC wavelength calibration is believed to be correct since it agrees with the known output spectra of the $CO_2$ laser. This agreement is a very encouraging result for both the NELC and the USC groups.

## Computer Simulation of Heat Flow in Calorimetry

The two-dimensional heat program TEMPS is now working. An initial run was made using insulated boundary conditions and actual laboratory sample parameters. The computed time rate of change of the surface temperature agreed within 5% with the results obtained from the theory used in the calorimeter measurements.

The three-dimensional heat program HEATING.3 has been received and is being made ready for use.

ABSORPTION COEFFICIENT

OF GaAs EMC 6012B

CALORIMETRIC DATA
at 300°K, USC

Emissivity Measurement
at 373°K by D. STIERWALT
NELC, San Diego

WAVELENGTH (μ)

37

ABSORPTION COEFFICIENT (CM⁻¹)

### f.2 Alkali Halide Surface Studies with Acoustic Probe Techniques
#### J. H. Parks, T. Colbert

A previous analysis[1] indicated the sensitivity and utility of acoustic surface wave propagation for the study of alkali halide surface properties. The primary emphasis during this quarter has been to develop these acoustic probe techniques. This effort has concentrated on achieving surface wave propagation on KCl surfaces, and beginning experiments to study the details of acoustic detection of infrared absorption at Y-cut Quartz surfaces.

#### I  Acoustic Wave Propagation on Alkali Halide Surfaces

The interdigital transducer used to excite surface acoustic waves relies on a piezoelectric coupling at the material surface on which it is placed. For this reason, it is not possible to generate surface waves on the centrosymmetric alkali halide surface by direct application of these transducers. Several methods can be applied to achieve wave propagation on non piezoelectric surface including

(a)  bulk wave to surface wave conversion,

(b)  growth of a piezoelectric crystal film (eg. sodium chlorate, lithium iodate, aluminum nitrite) on the material surface which then serves as a base for the transducer,

(c)  sputtering a thin film of zinc oxide on the non piezoelectric surface which becomes oriented during deposition and then serves as a transducer base,

(d)  coupling surface acoustic waves from a piezoelectric surface such as quartz through a fluid film interface to the surface of the non piezoelectric material.

Our initial attempt will be to excite surface propagation on alkali halide surfaces via fluid coupling from Y-cut Quartz. This method has been chosen because it demands the least sample preparation and handling. This is desirable since we plan to apply these techniques to study ultra high purity alkali halide surfaces.

A device to study the propagation behavior of acoustic waves which are fluid coupled to alkali halide samples is shown in Figure 1a. The precision micrometer head allows two acoustic transducers on individual Y-cut Quartz crystals to be brought into contact with a fluid interface between the Quartz and sample surfaces. In Figure 1b the mounting of the Quartz and sample is indicated to clarify the geometry of the fluid coupling interface. The fluid layer is held between the Quartz and sample by capillary

and does not extend further on the sample surface. As shown in Figure 1c, the acoustic wave initially propagates within this fluid layer and on the surfaces of the Quartz and sample. This wave will continue propagating beyond the fluid layer as a surface acoustic wave on the sample. This fluid coupling technique has been studied experimentally in References (2) and (3) and the propagation of layered waves is discussed in References (4) and (5) and more recently in Reference (6).

We are beginning an experimental study of surface wave propagation on KCl and NaCl samples. Initially the propagation behavior will be investigated using purchased material which has been polished to reduce surface irregularities to less than $\sim 1\mu$ size. Polishing techniques are being developed similar to those at NRL to allow us to prepare samples grown here at USC. These experiments will provide the following information:

(a)     The effects of disspersion and acoustic mode conversion introduced by layered structure, including the wave velocity as a function of fluid layer thickness,

(b)     acoustic frequency limitations caused by dispersion and also by attenuation of the material surface,

(c)     the stability of the fluid layer thickness.

The last point (c) is essential for the measurement of small, acoustic wave phase variations.[1] Mechanical vibrations and evaporation of the fluid which change the fluid thickness will introduce variations in the phase. For example, a phase variation of $\sim 10$ m rad corresponds to a change in the fluid layer thickness the order of $0.5\mu$. However, the phase change signal induced by sample absorption will have a time dependence which is significantly different from that of the layer thickness variation and will allow these effects to be separated. Another possibility for eliminating this uncertainty involves the use of two parallel acoustic waves propagating through the fluid layer structure. Any fluid thickness variation will affect both waves similarly and allow a null detection technique to eliminate these effects. The separation of these waves by a distance of $\sim 1$cm will isolate these waves from the coupling effects of thermal diffusion in the KCl, NaCl surface absorption experiments.

## II  Acoustic Detection of 10.6$\mu$ Radiative Absorption

Initial experiments have been performed to detect infrared absorption using acoustic wave techniques described in a previous report.[1] These

39

experiments are providing information on the possibility of using these
techniques to develop a new type of infrared detector, and also to develop
a method of measuring surface absorption which will be applied to alkali
halide materials. In these experiments $10.6\mu$ $CO_2$ laser radiation was
detected via surface wave propagation on Y-cut Quartz substrates. The
experimental setup consisted of a $CO_2$ laser which passed through a camera
shutter to generate pulses of 10 m sec to 100 m sec duration. An internal
aperature was used to control beam power and improve spatial mode quality.
To retain beam uniformity this radiation was not focused, and the detector
shown in Figure 2 surface was limited by a 3 mm diameter aperature. The
interdigital transducers generated a 120 MHZ surface wave of wavelength
$\lambda_s=25\mu$ which travelled through a pathlength of 2 cm (of which only 3 mm
was exposed to infrared radiation). The spatial distribution of the laser
intensity varied with power and limited the accuracy of determining the
actual $10.6\mu$ intensity probed by the $\sim 1$ mm wide acoustic beam to $\sim\pm 25\%$.
The mismatch of laser irradiated area ($\sim 7$ mm$^2$) and acoustic probed area
($\sim 3$ mm$^3$) reduced the effective infrared intensity depected by a factor of
$\sim 0.40$.

Figures 3a and 3b show representative data traces of detected
radiation for various laser powers and pulsewidths. The detected laser
power P, radiative pulsewidth $\tau_p$, the maximum phase variation $\Delta\phi_M$ are
indicated below for these data traces. The acoustic wave phase variation
was measured using a HP 8405A Vector Voltmeter and displayed on a
Tek 549 Storage Oscilloscope. The 1KHz bandwidth of the Vector Voltmeter
limited the detector response and accordingly the initial data includes only
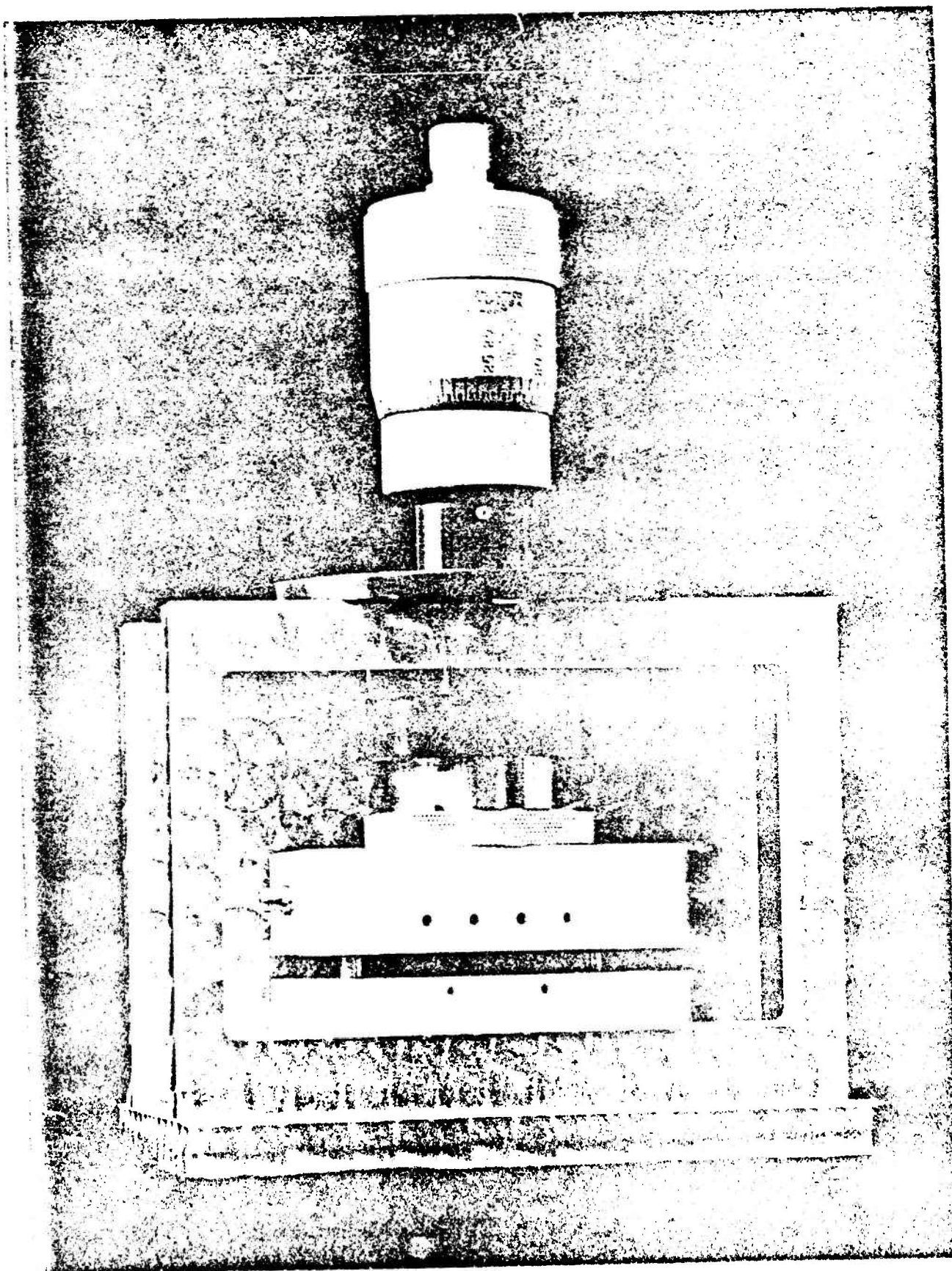$10.6\mu$ pulses having $\tau_p \geq 10$ m sec.

Figure 3a shows a small phase variation of $\Delta\phi_M \simeq 0.7$ mrad induced
by a $10.6\mu$ radiation with a timescale of 50 m sec per division. The
multiple exposure shown in Figure 3b represents a set of detected pulses
each having $P \simeq 0.2$ watt and different pulsewidths of $\tau_p=20$, 28, 47 and 90
m sec respectively. Each detector signal shows a linear ramp which is
characteristic of the temperature increase following a square radiation
pulsewidth. The effects of radial heat diffusion can be observed clearly
for the 90 m sec pulse as a slight curviture in the increasing signal trace.
The oscilloscope trace timescale is 50 m sec per division and the phase
variation scale is 1.5 mrad per division.

The detection of long radiative pulsewidths used in these initial
experiments cannot be analyzed by heat equation solutions which neglect

40

thermal diffusion terms. Although radial diffusion out of the acoustic beam path is $\leq 100$ m sec, the heat diffusion __perpendicular__ to the surface requires only $\sim 4\mu$ sec for heat to diffuse out of the depth, $d \simeq 25\mu$. This diffusion into the crystal bulk can reduce the sensitivity by a factor of $\sim 50$ for a 10 m sec radiation pulse; however short pulses $\leq 5\mu$ sec will be detected with full sensitivity. Analysis of the infrared detection data is presently underway using numerical solutions of the heat equation generated by Heating 3: An IBM Heat Conduction Program[7].

# REFERENCES

1. F. A. Kroger, J. H. Marburger et al. Electronic Sciences Laobratory, University of Southern California, "IR Window Studies", Quarterly Technical Report No. 3 (December-February 1973), AFCRL TR-73-0325, Contract No. F19628-72-C-0275, ARPA Order No. 2055 (29 September 1972).

2. W. C. Wang, P. Staecker and R. C. M. Li, Appl. Phys. Lett. 16 291 (1970).

3. P. Das, M. N. Araghi, Appl. Phys. Lett. 16, 293 (1970).

4. E. M. Ewing, W. S. Jardetzsky and F. Press, Elastic Waves in Layered Media (McGraw-Hill, New York, 1957) Chap. 4.

5. L. M. Brekhovskikh, Waves in Layered Media (Acedemic Press, Inc. New York 1960) pp. 61, ˜´6.

6. K. M. Lakin, D. Penunuri, Proceedings IEEE Symposium on Ultrasonics 1972, Catalogue No. 72. CHO 78-8SU.

7. W. D. Turner and M. Siman-Tov, Oak Ridge National Laboratory, ORNL-TM-3208, February 1971.
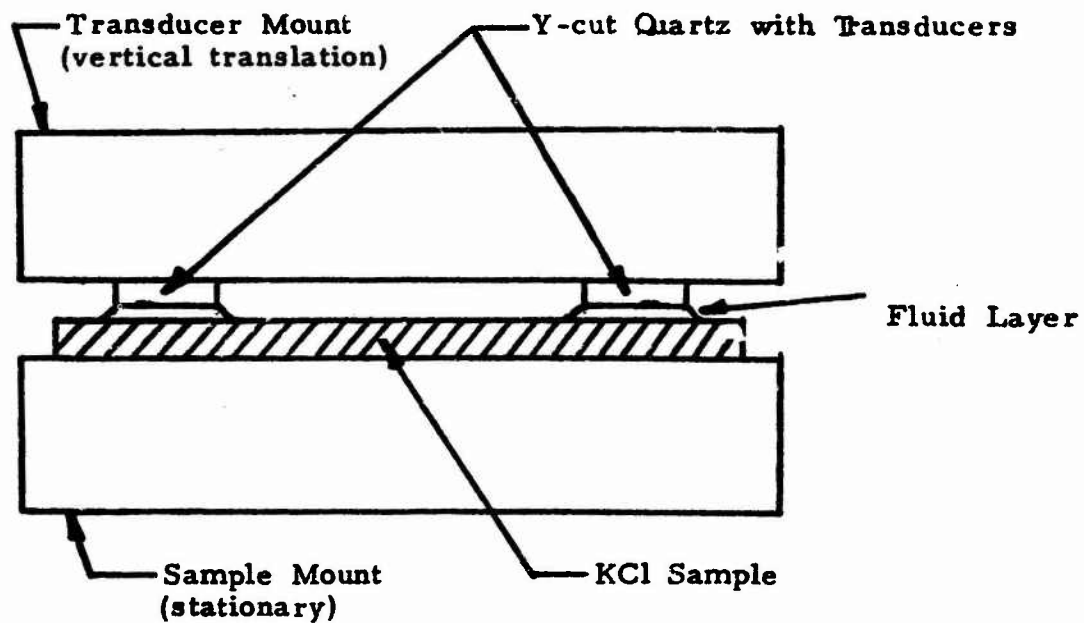
Figure 1a. Fluid coupling device showing the translating transducer mount (upper) and the stationary sample mount (lower)

43

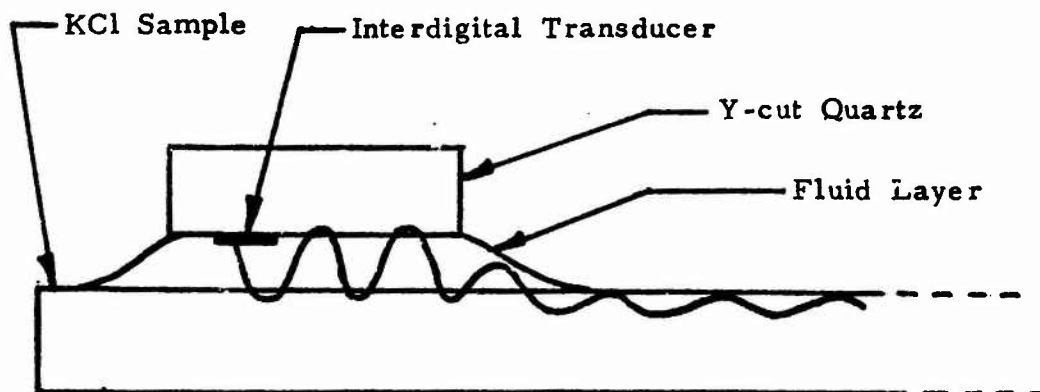Figure 1b. Fluid coupling arrangement of transducers and sample



Figure 1c. Fluid coupling schematic showing acoustic wave propagation
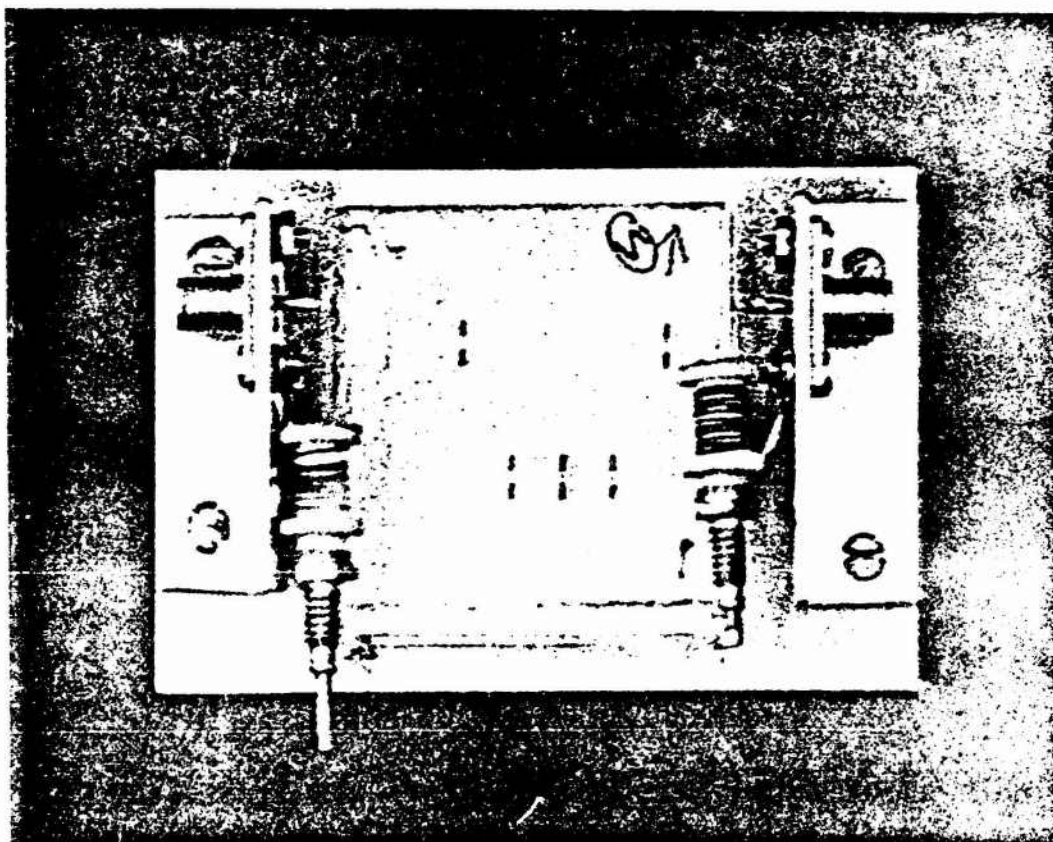
44

Figure 2. The acoustic surface wave propagates between the two upper transducers separated by 2 cm. These transducers are on a 1.5 inch square substrate of Y-cut crystal quartz which is bonded to an electrode connector holder.
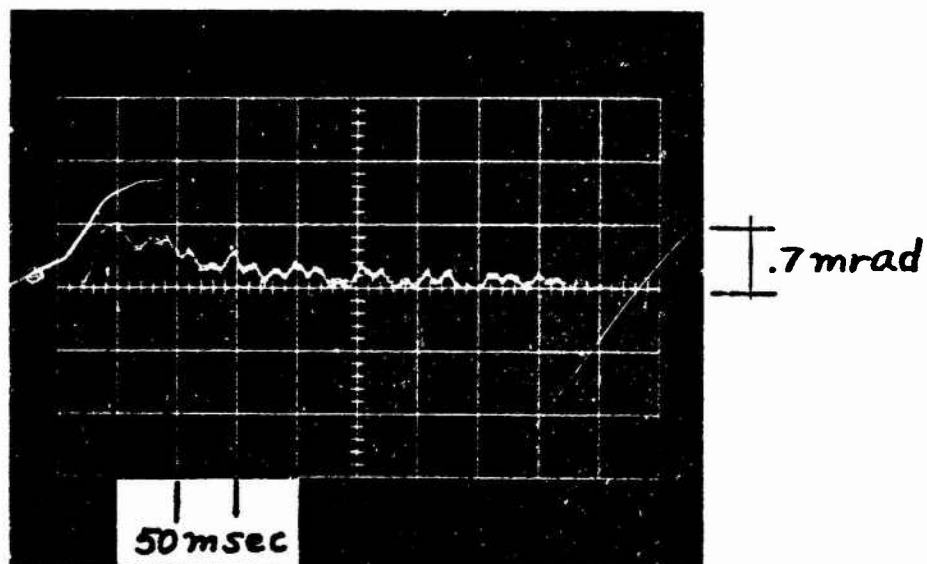
45

Figure 3a.  Acoustic wave phase signal induced by
the absorption of a 50 mwatt pulse having
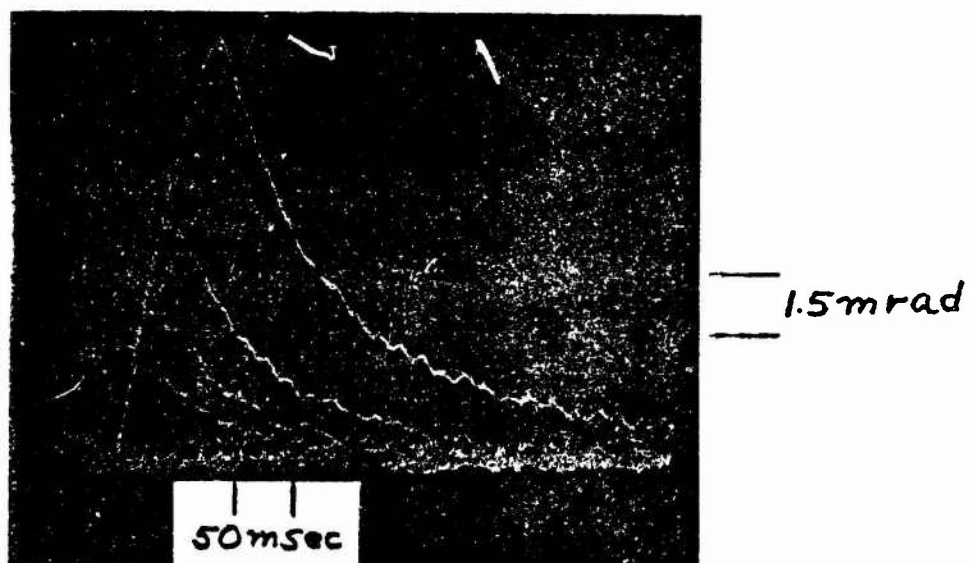a pulsewidth of 20 msec.



Figure 3b.  Multiple exposure showing acoustic wave
phase signals induced by the absorption
of .2 watt pulses having pulsewidths of
20, 28, 47, and 90 msec. respectively.

## g.1 Characterization of Optical Performance of IR Window Systems

### Martin Flannery, J. H. Marburger

In the last quarterly report we described an approximate method for treating window birefringence from a narrow laser beam if the beam could be approximated by the superposition of several circularly symmetric beams clustered near the window's center. The method is simply to consider each circular piece of the beam to be centrally located in a disc and to solve for the temperature distribution and resulting stresses on that disc, and finally to superpose the solutions for all pieces of the beam. The object of the approximation was to find relatively accurate solutions of slightly asymmetric beams without the necessity of using a general thermoelastic computer program.

It was decided to use this approximation to include birefringence in a further investigation of the beam slewing reported for a KCl window by Dr. L. Skolnik of AFCRL. A central scan of the laser beam used in these experiments was provided by Dr. Skolnik as described in the 2nd Quarterly Report.

To match this central scan we developed the following intensity profile:

(1) $\quad I(x,y)/I_o = i(r) + i(s)$

(2) $\quad i(r) = A(e^{-\omega r^2} - e^{-\omega a^2}) + \begin{cases} Br^2(C-r)^4 & : r < C \\ 0 & : r \geq C \end{cases}$

(3) $\quad i(s) = C_1(e^{-\omega_1 s^2} - e^{-\omega b^2})$

(4) $\quad s = (x-x_o)^2 + y^2$

where $r=0$ is the window center, $r=a$. The window edge and $i(r)$ the central beam. For the secondary beam, $i(s)$, centered at $r = x_o$, we will assume $C_1 \ll A$ and that it covers a disc of radius $b = a+x_o$. Both pieces of the beam were adjusted to have zero intensity at the edges of their respective discs so the heat equation for each disc could be solved with the boundary conditions $T(edges) = 0$.

In what follows we will generally only work out the solutions for $i(r)$ since the solutions for $i(s)$ can be gotten from them by a suitable change of parameters.

Also all distances are assumed to be normalized to d, which is usually taken to be the diameter of the aperture used in the computer diffraction program (and which may be taken as d = a, but d < a is often chosen to save computer time on very narrow beams).

## I    THE HEAT EQUATION

To get sufficient characterization of the window performance it seems sufficient to solve the heat equation for short times, assuming the diffusion term is zero, and for the steady-state case. For simplicity, we will use the boundary conditions T (edges) $\equiv 0$.

In terms of the normalized time $\tau = kt/d^2$, where k is the thermal diffusion coefficient and with the temperature normalized to $T_o = \beta I_o/k_{th}$, the general heat euqation is:

(5)    $d_\tau T = \nabla^2 T + Q/k_{th} T_o$

For short times we have the solution

(6)    $T = \dfrac{Q}{k_{th} T_o} \quad \tau = \tau \, I(x,y) /I_o$

The fact that this solution is linear in time will result in the whole phase delay through the window being linear in time and allow us to calculate many time steps with relatively little work.

For the steady state case we must solve each circular beam separately to preserve its circular symmetry. With the aid of the Greens function for a circular symmetric heat distribution,

(7)    $G(r|r^1) = -4\pi \ell nr \quad ; \quad r > r^1$

$\qquad\qquad = -4\pi \ell nr^1 \quad ; \quad r < r^1$

we find the steady-state solution is:

(8)    $T(r) = \dfrac{1}{4\pi} \displaystyle\int_0^a G(r|r^1) \; i \, (r^1) \; r^1 dr^1$

and similarly for i(s). There is no difficulty in integrating (8) for the intensities (2) and (3), but the polynomial in (2) does produce a lot of terms so we won't write the solution here. The Gaussian terms in (2) and (3) produce a term which is most

48

easily written in terms of the exponential integral function.

## II   OPTICAL ABERRATION

For a window of thickness h and refractive index n, the optical path length is $\ell = nh$. When the window is heated or strained the change in the optical path length to first order is:

(9)   $\Delta \ell = (n_o - 1) \Delta h + h \, \Delta n$

where the factor $(n - 1)$ accounts for the change in path length on expansion as the new path length through the window minus the old path length through the air.

There are a large number of effects that can produce changes in h and $n_o$ but we will consider only the following:

(A)   Free thermal expansion in the direction perpendicular to the plane of the window:

(10)   $\Delta h_\alpha = \alpha h \, T_o \, T_t$

where   $\alpha$ is the linear expansion coefficient and $T_t$ is the total temperature

(B)   Bulging in the direction perpendicular to the window due to the partially constrained expansion in the plane of the window is given by:

(11)   $\Delta h_b = -\nu h a T_o (\sigma_{rr} + \sigma_{\theta\theta})$

which follows from Hook's law, and where the stresses have been normalized to $\alpha E \, T_o$, E is Young's modulus, $\nu$ Poisson's ratio. For an isotropic cylindrically symmetric temperature distribution these normalized stresses are:

(12)   $\sigma_{rr} = g(a) - g(r)$

(13)   $\sigma_{\theta\theta} = g(a) + g(r) - T$

(14)   $\sigma_{rr}(0) = \sigma_{\theta\theta}(0) = g(a) - T(0)/2$

where

(15)   $g(r) = \dfrac{1}{r^2} \int_0^r T \, r \, dr$

49

Using these expressions in equation (11) and ignoring a constant term we get the constrained bulging as:

(16) $\quad \Delta h_b = \nu h \, \alpha \, T_o T_t$

if we again include all the beam components.

The refractive index will change because of its normal temperature dependence and the stress-optic effect. Using Hook's Law we can write the incremental indicatrix (in terms of the stresses) for a cylindrically symmetric window as:

(17) $\Delta B_{rr} = n_r^{-2} - n_o^{-2} = (p_{11} + 2p_{12}) \, \alpha \, T_o T + b_{\parallel} \sigma_{rr} + b_{\perp} \sigma_{\theta\theta}$

(18) $\Delta B_{\theta\theta} = n_\theta^{-2} - n_o^{-2} = (p_{11} + 2p_{12}) \, \alpha \, T_o T + b_{\parallel} \sigma_{\theta\theta} + b_{\perp} \sigma_{rr}$

where the p's are the strain-optic coefficients and the b's are stress-optic coefficients.

(C)    The normal thermal changes in the refractive index are usualy expressed in terms of the experimental value

(19) $\quad \dfrac{dn}{dT}\bigg|_{\sigma=0} = \dfrac{dn_o}{dT} - \dfrac{n_o^3}{2}(p_{11} - 2 p_{12}) \, \alpha$

so the isotope terms in equations (17) and (18) can be included here:

(20) $\quad \Delta n_{\sigma=0} = \dfrac{dn}{dT}\bigg|_{\sigma=0} T_o \, T_t$

(D)    The remaining anisotropic terms in equations (17) and (18) are the stress-birefringence effect. There will be a set of these equations for each circular piece of the beam, but in order to get the total incremental indicatrix we must transform them to the same coordinate system, which we choose to be the cartesian xy-system.

The anisotropic part of the refractive indices for the two principle waves cannot be found by diagonalizing the total indicatrix at each point in the window. If the eigenvalues are $\Delta B_i$, then using the relationship

50

(21)  $\Delta B_i = n_i^{-2} - n_o^{-2} \cong 2(n_i - n_o)/n_o^3$

we can write the anisotropic increments in the refractive index as:

(22)  $\Delta n_{1,2} \cong - n_o^3 \, \Delta B_{1,2}/2$

The total path length changes can now be written as

(23)  $\Delta \ell_{1,2} = (n_o - 1) \, (\Delta h_a + \Delta h_b) + h \Delta n_{\sigma=0} + h \Delta n_{1,2}$

from equations (9), (10), (16), (20) and (22). The isotropic part is characterized by the single constant G:

(24)  $\Delta \ell_o = h T_o \left[ (n_o - 1) \, (1 + \nu) \, \alpha + \dfrac{dn}{dT}_{\sigma = 0} \right] T_t \, \tau = G \, \tau$

where we have pulled the dimensionless time $\tau$ out of the temperature in the case of short times and for long times set $\tau = 1$. For the anisotropic part it will be convenient to incorporate the factor of h in (23) and the factor of $n_o^3/2$ in (21) into the stress optic coefficients of equations (17) and (18), so (23) becomes,

(25)  $\Delta \ell_{1,2} = \Delta \ell_o - \Delta B_{1,2} \, \tau$

The anisotropic part is characterized by the two constants

(26)  $b_\parallel = \alpha n_o^3 h T_o \, (p_{11} - 2 \, \nu p_{12}) \, /2$

(27)  $b_\perp = \alpha n_o^3 h T_o \, ( (1 - \nu) \, p_{12} - \nu p_{11}) \, /2$

Thus the whole problem is characterized by three material constants.

## III   DISCUSSION

We will make a computer parameter study of the three material constants including a comparison for G along with those of the slab beam reported in the 2nd quarterly report. We will also look at the birefringence alone as well as in combination with the isotropic effect.

51

In the next quarter we will have available a general heat equation program from Oak Ridge National Labs so we may compare the accuracy of our approximate solution of the heat equation with the exact solution. Equally we hope to either acquire or write a thermoelastic computer program to solve the thermoelastic problem in simple disc windows of isotropic or cubic material with general temperature distributions.

## 3. DISCUSSION

Additional absorption measurements on high purity melt grown GaAs samples prepared by horizontal bridgeman and float-zone techniques have convinced us that there is a lower limit to the absorption coefficient at 10.6$\mu$m for such samples of about $\beta \approx .008\mu$m. The similarity of the absorption spectra in the 9 to 11 $\mu$m region for all samples measured is very striking, considering the very different materials processing techniques represented in our selection. Our temperature dependent measurements have not yet been completed.

The absorption coefficient of one of the Bell and Howell GaAs samples has been decreased appreciably by annealing as anticipated by Prof. Copley, but the reduced absorption spectrum did not fall below the lower limits observed in other higher quality samples.

We are undertaking accurate measurements of the dielectric constant $\epsilon$ of GaAs as there seems to be some ambiguity in available values for this parameter. Prof. Hellwarth has stressed the importance of accurate knowledge for $\epsilon$ for comparison of theoretical expressions with experiment.

The acoustic surface wave technique for measuring absorption coefficients has been developed to the point where preliminary experiments to determine the 10.6 $\mu$m absorbance of quartz have been performed. Extraction of the absorption coefficient from the data requires numerical analysis, now in progress. Quartz is used in these initial experiments because the acoustic wave technology is well developed for this material. During this period, a device has been fabricated to launch and detect acoustic waves on alkali halide samples. Samples of low $\beta$ KCl with high quality surfaces have been ordered from Janos Optical Corp. (Vermont) to expedite this project. We plan to develop an in-house capability for preparing alkali halide surfaces of sufficient quality for the acoustic wave technique.

KCl crystals have been grown from the ultra pure material described in previous reports. The apparent quality of the crystals (by visual inspection) is improving as experience with the apparatus accumulates. Insufficient data on absorption coefficients has been obtained for these samples to report a meaningful number.

The experimental work on high temperature transport properties of CdTe, including self diffusion of Cd and Te, and high temperature Hall effect, has been completed. While the results are being analyzed, steps are being taken to obtain

material for studies of the electrical and optical properties at lower temperatures. The material will probably be purchased from II-VI Inc. (Pennsylvania).

Theoretical work during this period included the development of further checks on the approximate multiphonon absorption theories using exact moment calculations reported previously. Some of this work was reported at the NBS-ASTM Symposium on Damage in Laser Materials in May.

The superposition approximation for acentric stress distributions reported previously has been exploited during this period in a calculation of the influence of stress induced birefringence on thermal slewing of acentric beams. The theory is strictly applicable only to mechanically isotropic substances, but we believe that it will lead to reasonable quantitative estimates for the size of the effect in cubic anisotropic substances such as the alkali halides. Difficulties with the computer driven plotter at our computation facility prevented us from including the results of the theory in this report.